

Gene therapy restores dopamine transporter expression and ameliorates pathology in iPSC and Mouse Models of Infantile Parkinsonism

Authors

Joanne Ng^{1,2+}, Serena Barral^{2+*}, Carmen De La Fuente Barrigon³, Gabriele Lignani⁴, Fatma A. Erdem^{2,6}, Rebecca Wallings⁷, Riccardo Privolizzi^{1,2}, Giada Rossignoli², Haya Alrashidi³, Sonja Heasman², Esther Meyer², Adeline Ngoh², Simon Pope⁸, Rajvinder Karda¹, Dany Perocheau¹, Julien Baruteau^{1,3}, Natalie Suff^{1,9}, Juan Antinao Diaz¹, Stephanie Schorge^{4,5}, Jane Vowles¹⁰, Lucy R. Marshall¹¹, Sally A. Cowley¹⁰, Sonja Sucic⁶, Michael Freissmuth⁶, John R. Counsell¹², Richard Wade-Martins⁷, Simon J. R. Heales⁸, Ahad A. Rahim⁵, Maximilien Bencze^{12,13}, Simon N. Waddington^{1,14**}, Manju A. Kurian^{2,15#}

Affiliations

1. Gene Transfer Technology Group, EGA-Institute for Women's Health, University College London, London, WC1E 6HX, UK.
2. Developmental Neurosciences, Zayed Centre for Research into Rare Disease in Children, GOS-Institute of Child Health, University College London, London, WC1N 1DZ, UK.
3. Genetics and Genomic Medicine, GOS-Institute of Child Health, University College London, London, WC1N 1EH, UK.
4. Clinical and Experimental Epilepsy, Queen Square Institute of Neurology, University College London, London, WC1N 3BG, UK.
5. Pharmacology, School of Pharmacy, University College London, London, WC1N 1AX, UK.
6. Institute of Pharmacology and Gaston H. Glock Laboratories for Exploratory Drug Research, Centre of Physiology and Pharmacology, Medical University of Vienna, 1090 Vienna, Austria.
7. Oxford Parkinson's Disease Centre, Department of Physiology, Anatomy and Genetics, University of Oxford, Oxford, OX1 3PT, UK.
8. Neurometabolic Unit, National Hospital for Neurology and Neurosurgery, Queen Square, London, WC1N 3BG, UK.
9. Department of Women and Children's Health, King's College London, London, WC2R 2LS, UK.
10. James Martin Stem Cell Facility, Sir William Dunn School of Pathology, University of Oxford, Oxford, OX1 3RE, UK.
11. Infection, Immunity, Inflammation, GOS-Institute of Child Health, University College London, London, WC1N 1EH, UK.

1 12. Developmental Neurosciences, GOS-Institute of Child Health, University College London, London, WC1N
2 1EH, UK.

3 13. University Paris Est Creteil, INSERM, IMRB, 94000 Creteil, France.

4 14. Wits/SAMRC Antiviral Gene Therapy Research Unit, Faculty of Health Sciences, University of the
5 Witwatersrand, 2193 Johannesburg, South Africa.

6 15. Department of Neurology, Great Ormond Street Hospital for Children, London, WC1N 3JH, UK.

7

8 + these authors contributed equally to the manuscript

9 # these authors contributed equally to the manuscript

10 ***Corresponding authors:**

11 Professor Simon N. Waddington –Gene Transfer Technology Group, EGA-Institute for Women's Health,
12 University College London, WC1E 6HX London, UK – Email: s.waddington@ucl.ac.uk

13 Dr Serena Barral – Developmental Neurosciences, Zayed Centre for Research into Rare Disease in Children,
14 GOS-Institute of Child Health, University College London, WC1N 1DZ London, UK – Email: s.barral@ucl.ac.uk

15

One Sentence Summary:

Viral vectors restore dopamine transporter function and ameliorate neuropathology in iPSC-derived neurons and a mouse model of infantile parkinsonism

Abstract

Most inherited neurodegenerative disorders are incurable, and often only palliative treatment is available. Precision medicine has great potential to address this unmet clinical need. We explored this paradigm in Dopamine Transporter Deficiency Syndrome (DTDS), caused by biallelic loss-of-function mutations in *SLC6A3*, encoding the dopamine transporter (DAT). Patients present with early infantile hyperkinesia, severe progressive childhood parkinsonism and raised cerebrospinal fluid dopamine metabolites. The absence of effective treatments and relentless disease course frequently leads to death in childhood. Using patient-derived induced pluripotent stem cells (iPSCs), we generated a midbrain dopaminergic (mDA) neuron model of DTDS which exhibited marked impairment of DAT activity, apoptotic neurodegeneration associated with TNF α -mediated inflammation and dopamine toxicity. Partial restoration of DAT activity by the pharmacochaperone pifithrin- μ , was mutation-specific. In contrast, lentiviral gene transfer of wild-type human *SLC6A3* complementary DNA restored DAT activity and prevented neurodegeneration in all patient-derived mDA lines. To progress towards clinical translation, we utilized the knockout mouse model of DTDS which recapitulates human disease, exhibiting parkinsonism features, including tremor, bradykinesia and premature death. Neonatal intracerebroventricular injection of human *SLC6A3* using an adeno-associated virus (AAV) vector provided neuronal expression of human DAT which ameliorated motor phenotype, lifespan and neuronal survival in the substantia nigra (SN) and striatum, though off-target neurotoxic effects were seen at higher dosage. These were avoided with stereotactic delivery of AAV2.SLC6A3 gene therapy targeted to the midbrain of adult knockout mice, which rescued both motor phenotype and neurodegeneration, suggesting that targeted AAV gene therapy might be effective for patients with DTDS.

Introduction

Most neurodegenerative disorders lack effective disease-modifying treatments. This leads to substantial morbidity, increased risk of mortality and considerable socioeconomic burden. With deeper understanding of the underlying pathogenic processes, targeted precision medicine strategies are increasingly becoming a clinical reality (1,2).

Dopamine transporter (DAT) is highly expressed in pre-synaptic midbrain dopaminergic (mDA) neurons, where it re-uptakes released dopamine (DA) from the synaptic cleft. It is a key regulator of the amplitude and duration of dopaminergic transmission (6). To date, 29 cases of DTDS have been published (3-5,7-13) and a further 17 are unpublished, referred to our centre between 2015 and 2020. Since many reported patients have been misdiagnosed with cerebral palsy (4), the true incidence is likely to be higher. DTDS presents as a progressive movement disorder characterized initially by infantile-onset hyperkinesia, with features of dystonia, choreoathetosis, ballismus, orolingual dyskinesia and recurrent oculogyric crises. Life-threatening status dystonicus is commonly reported. Severe parkinsonism with akinesia, rigidity, tremor and hypomimia develops in late childhood or early adolescence. Analysis of neurotransmitter concentrations in cerebrospinal fluid (CSF) characteristically reveals a raised concentration of the dopamine metabolite, homovanillic acid (HVA) but a normal concentration of serotonin metabolite 5-hydroxyindoleacetic acid (5-HIAA), leading to a pathologically increased CSF HVA:HIAA ratio. The relentless disease course and lack of effective treatments frequently leads to premature death in the first or second decade of life, usually secondary to respiratory complications.

Very little is known about the cellular progression of DTDS in the central nervous system. Progressive changes were measured by single-photon emission computed tomography (SPECT) imaging with ioflupane (1123) (DaTscan) over an 8 year interval in a patient with atypical DTDS (7). Although this is suggestive of progressive nigrostriatal neurodegeneration, post-mortem data from patients with DTDS has not yet been available to confirm this clinical observation. To date, our limited understanding of cellular mechanisms underpinning DTDS pathogenesis has hindered the development of effective disease-modifying or curative therapies.

Here, we have utilized a patient-derived induced pluripotent stem cell (iPSC) midbrain dopaminergic (mDA) neuronal system in tandem with a murine model of disease to investigate clinically translatable precision medicine strategies for patients with DTDS.

Results

Loss of DAT function and dysregulated dopamine metabolism is evident in mDA neurons derived from patients with DTDS.

Using a patient-derived mDA model, we first explored the effect of mutant DAT protein on neuronal function, comparing patient lines to age-matched and CRISPR-corrected controls.

iPSC lines were generated from dermal fibroblasts of patient with DTDS with homozygous missense mutations in *SLC6A3* (Patient 1: c.1103T>A, p.L368Q; Patient 2: c.1184C>T, p.P395L) (3). Control iPSCs were similarly generated from an age-matched healthy individual. An isogenic control line was created by CRISPR-Cas9 correction of the c.1184C>T variant in Patient 2. Genomic DNA sequencing confirmed that all patient-derived iPSC lines maintained their specific homozygous *SLC6A3* mutation, with successful correction of the mutation in the isogenic control (fig. S1A). All iPSC lines exhibited pluripotency and maintenance of genomic integrity (fig. S1B-H).

Given the specific expression profile of DAT (6), patient-derived iPSC lines were then differentiated into mDA neurons (14, 15). After 11 days of differentiation, comparable high numbers of mDA progenitors were present in both DTDS patient and control lines (fig. S2A,B) with typical midbrain precursor gene expression profiles (fig. S2C). After 65 days of differentiation, mature mDA neurons showed a typical gene and protein expression profile, characteristic dopaminergic cell firing pattern and evidence of dopamine release (fig. S3A-E).

In order to determine the effect of biallelic *SLC6A3* mutations on transporter function, we analyzed DAT activity in the DTDS neuronal cell model. Uptake of tritiated [³H]dopamine in patient 1 and 2 lines was significantly reduced ($P = 0.0397$, $P = 0.0048$ respectively, and Patient 2 vs CRISPR $P = 0.0033$), indicating a marked disruption of DAT activity (Fig. 1A). The impact of impaired transporter function on dopamine uptake and homeostasis was then evaluated by measurement of extracellular dopamine metabolites. High performance liquid chromatography (HPLC) revealed significantly increased concentrations of HVA and 3,4-Dihydroxyphenylacetic acid (DOPAC) ($P < 0.0001$, $P = 0.0002$ respectively, and Patient 2 vs CRISPR $P = 0.0487$) (Fig. 1B,C).

We sought to establish whether the observed loss of DAT function was secondary to reduced gene expression or impaired protein synthesis. There was no change in *SLC6A3* mRNA expression (fig. S4A) but increased DAT protein concentration was evident in patient-derived mDA neurons (Fig. 1D, S4B,4C).

We then analyzed the impact of DAT dysfunction and dopaminergic dysregulation on other key enzymes involved in dopamine synthesis. Although patient-derived neuronal cultures showed an overall significant reduction in total tyrosine hydroxylase (TH) protein expression ($P = < 0.0001$, $P = 0.0065$ respectively, and Patient 2 vs CRISPR $P = 0.0238$) (Fig. 2A; S5A), there were no differences in TH gene and protein expression specifically in the mDA neuronal subpopulation (Fig. 2B; S5B). Furthermore, no differences in aromatic L-amino acid decarboxylase (AADC) mRNA and protein expression were found (Fig. 2A,C; S5C).

In contrast, analysis of key enzymes involved in dopamine catabolism revealed a disease-specific reduction in monoamine oxidase A and B (MAO-A/B) gene and protein expression (Fig. 2D-F; S5D,E). In our neuronal cultures, MAO-A was widely expressed in both mDA neurons and glial cells (Fig. 2G) with significant reduction in MAO-A concentrations in patient-derived mDA neurons ($P = 0.0019$, $P = 0.0031$ respectively, and Patient 2 vs CRISPR $P = 0.0226$) (Fig. 2H). Unlike MAO-A, MAO-B expression was only detected in GFAP positive cells (Fig. 2G) suggesting a disease-specific reduction of this enzyme in glial cells. We sought to determine whether aberrations in MAO-A and MAO-B were evident in CSF from patients with DTDS. Immunoblotting of patient CSF revealed no difference in MAO enzyme concentrations (fig. S5F-H).

Impairment of DAT activity in DTDS is associated with neurotoxicity and apoptotic neurodegeneration

We identified a marked reduction of total neurons in patient-derived lines, compared to both age-matched and isogenic controls (Fig. 3A,B; S6), and as a result, a proportionate patient-specific reduction of TH⁺ cells (Fig. 3B; S6). Apoptosis, as measured by cleaved caspase-3 immunofluorescence, was significantly increased in neurons and more specifically in mDA neurons, but not in glial cells (MAP2/cCASP3/DAPI: $P = 0.0039$, $P = 0.0014$ respectively, and Patient 2 vs CRISPR $P = 0.0013$; TH/cCASP3/DAPI: $P = 0.0025$, $P = 0.0001$ respectively, and Patient 2 vs CRISPR $P < 0.0001$) (Fig. 3C,D; S7).

Further work was undertaken to elucidate potential mechanisms leading to apoptotic programmed cell death and neuronal loss. We firstly investigated the role of dopamine toxicity in DTDS pathogenesis as raised dopamine metabolites are observed in both patient CSF and the patient-derived neuronal cell model. Formation of carbonyl species, a marker of dopamine-triggered stress response, was significantly increased in both DTDS patient-derived neuronal cultures and age-matched dopamine-treated controls, when compared to isogenic and dopamine-untreated controls (Control vs Control DA $P = < 0.0001$, $P = 0.0003$, $P = 0.0039$, and Patient 2 vs CRISPR $P = 0.0292$) (Fig. 3E,F).

Given the established pathogenic role of neuroinflammation in neurodegenerative disorders (16), we utilized the in vitro mDA model to investigate the effect of proinflammatory cytokines, in the context of dopamine toxicity secondary to extracellular dopamine accumulation (17-19). Despite the presence of GFAP-positive glial cells in both patient- and control-derived neuronal cultures (Fig. 4A; S8A), exposure to lipopolysaccharide (LPS) and dopamine did not induce cell death. There was no difference in cell membrane permeability in patient lines when compared to controls (Fig. 4B). Due to the relative immaturity of the glial system in our iPSC-derived mDA model, it is not surprising that we

1 did not see LPS-stimulated cytokine release. We therefore artificially exposed our mDA neuronal
2 model to the glial cell-derived proinflammatory cytokines, TNF α and IL-1 β , with and without the
3 addition of dopamine. Whereas TNF α and IL-1 β did not affect cell death per se, concurrent treatment
4 with dopamine led to a disease-specific significant increase in membrane permeability and caspase-
5 dependent cell death (TNF α : $P = 0.0314$ and $P = < 0.0001$ respectively, IL-1 β $P = < 0.0001$ and $P =$
6 0.0029) (Fig. 4C,D).

7 Following these findings, we sought to determine whether there was evidence of proinflammatory
8 cytokine release in DTDS by measuring cytokine concentrations in CSF of 5 patients. All had raised
9 CSF HVA (mean CSF HVA:HIAA ratio 10.8, normal range 1.3-4.0) (20). Overall, there was no
10 difference in TNF in patients with DTDS compared to pediatric controls (fig. S8B). However, we
11 identified raised TNF in two patients with more advanced disease (age 6 and 16 years), in contrast to
12 those with early stage disease ($n = 3$, all aged < 2 years) (fig. S8C).

13 ***DAT function can be rescued with pifithrin- μ and lentiviral gene transfer in the patient-derived*** 14 ***mDA neuronal model***

15 Having established disease-specific parameters in the DTDS iPSC-derived mDA model, we utilized
16 the model to validate targeted treatments for DTDS. Most missense variants in DTDS are associated
17 with loss of transporter function, due to protein folding defects, retention in the endoplasmic reticulum
18 (ER) (21-23), and reduced surface expression of mature glycosylated transporter (3-5). Therefore,
19 we tested whether the Heat Shock Protein 70 (HSP70) inhibitor pifithrin- μ could rescue defective
20 protein folding and restore DAT function in vitro (21). Mature mDA neurons at Day 65 were treated
21 for 24 hours with pifithrin- μ , before measuring uptake of tritiated dopamine. Neurons derived from
22 Patient 1 showed a significant two-fold increase in DAT activity ($P = 0.0006$), reaching 35% of mean
23 dopamine uptake activity observed in control lines with no overall increase in total DAT protein (Fig.
24 5A; S9A,B). No increase in DAT activity with pifithrin- μ was observed for Patient 2 (Fig. 5A).

25 Given the mutation-specific effects of pifithrin- μ treatment, we sought to develop a gene therapy
26 approach, applicable to a broader range of patients with DTDS. A lentiviral construct was generated
27 expressing human *SLC6A3* gene under the transcriptional control of the neuron-specific promoter,
28 human synapsin (hSYN1) (fig. S9C,D). Patient derived mDA precursors were transduced at Day 24
29 of differentiation and analyzed at Day 65 of derived maturity. Lentiviral gene transfer led to restoration
30 of dopamine uptake (Fig. 5B). Despite this recovery of DAT activity, we did not observe normalization
31 of dysregulated MAO-A and MAO-B enzyme concentrations by Day 65 (fig. S9E-G). Nonetheless,
32 rescue of DAT function by gene therapy successfully halted neuronal loss, and more specifically,
33 prevented dopaminergic neurodegeneration (Fig. 5C,D).

Proof of concept gene therapy of DAT knockout mice by neonatal intracerebroventricular gene transfer

In preparation for in vivo preclinical gene therapy, we injected adeno-associated virus serotype 9 (AAV9) vector encoding GFP under transcriptional control of a truncated hSyn1 promoter (fig. S10A) (2×10^{11} vector genomes (vg), $n = 4$: 1 male, 3 females from a single litter) into the lateral ventricle of neonatal wildtype mice. At 35 days, GFP expression extended bilaterally, from the prefrontal cortex to cerebellum and was, notably, present in mDA neurons (fig. S10B,C).

We established baseline phenotype readouts in a previously-characterized DAT knockout mouse model (24,25). Consistent with previous studies, all knockouts exhibited poor weight gain (Fig. 6A), displaying hyperlocomotor activity by P21 (Supplementary Video 1) with 59% developing tremor, bradykinesia and weight loss (Supplementary Video 2), reaching humane endpoint by P35 ($n = 10$, 4 males, 6 females) (Fig. 6B).

We generated an AAV9 vector for human DAT expression under transcriptional control of a truncated hSyn1 promoter (fig. S10D). At P0, DAT knockout pups received intracerebroventricular injection of vector (2.25×10^{10} vg per pup, $n = 13$: 7 males, 6 females from 4 litters). Uninjected wildtype littermates ($n = 12$: 5 males, 7 females from 5 litters) and knockouts ($n = 17$: 9 males, 8 females from 7 litters) served as controls. Treated knockouts were significantly heavier than surviving untreated knockouts ($P = 0.001$) (Fig. 6A). 10 out of 17 untreated knockouts required euthanization before 35 days; the remainder survived until tissue collection at 365 days. All treated knockouts and wildtype mice survived to the collection timepoints (Fig. 6B). Untreated knockouts were hyperactive, travelling significantly further distances (at 3, 6, 9, 12 months $P = < 0.0001$) and with less central zone time in open field tests ($P = < 0.0001$); treated knockouts were indistinguishable from wild type littermates in both distance travelled and central time (Fig. 6C,D). Knockouts had a significantly prolonged descent time on the vertical pole test (at 3, 6, 9, 12 months $P = < 0.0001$) and made significantly more foot faults (3 months $P = < 0.0001$, 6 months $P = 0.0015$, 9 months $P = 0.0003$, 12 months $P = < 0.0001$); the performance of treated knockouts was indistinguishable from wildtype mice (Fig. 6E,F). Treated knockouts did not develop parkinsonism, unlike their untreated knockout littermates (Supplementary Video 3).

Treated knockouts expressed hDAT bilaterally from the prefrontal cortex to cerebellum including striatum and midbrain, where DAT is physiologically expressed (Fig. 6G). Whole brain homogenate from untreated knockouts had significantly reduced dopamine concentrations ($P = < 0.0001$) with raised DOPAC and HVA compared with wildtype mice; these differences were reversed, but not normalized, in treated knockouts (Fig. 6H). Gene therapy ameliorated both dopaminergic and striatal

neurodegeneration (Fig. 6I,J). Patch clamp electrophysiology of medium spiny neurons in the dorsal striatum revealed the presence of two different populations in wildtype mice, exhibiting high and low firing rates and only high-firing rate neurons were detected in the untreated knockouts AAV9.SLC6A3 treatment of knockouts restored the bimodal firing distribution (Fig. 6K; S11) ($\chi^2 P = 0.003$).

To attempt to fully restore dopamine homeostasis and neurotransmitter profile, a second knockout group received a ten-fold higher dosage of intracerebroventricular AAV9.SLC6A3 gene therapy at P0 (2.25×10^{11} vg per pup, $n = 12$: 7 males, 5 females from 4 litters) by injection. Treated mice were heavier than untreated knockouts, however 50% of them developed unexpected, early tremor, bradykinesia and weight loss necessitating euthanasia by P35 (fig. S12A,B). The remainder were indistinguishable, on motor behavioral testing, from wildtype and survived to sacrifice at 365 days (fig. S12C-F, Supplementary Video 4). Bilateral hDAT expression was observed throughout the brain; however mDA transduction was not increased compared to lower dose cohort (fig. S12G-I). Furthermore, despite restoration of HVA concentrations and correction of neurodegeneration (fig. S12J-L), there was cortical cell loss and vacuolation with marked GFAP expression in the cerebral cortex (fig. S12M).

Preclinical gene therapy for DTDS – targeted delivery to the substantia nigra for future clinical translation

In order to move towards translation, we further developed vector delivery to model clinical application and restrict expression to dopaminergic neurons by intraparenchymal stereotactic delivery. We selected AAV2 capsid which exhibits restricted spread after central nervous system delivery (26) and has precedent in gene therapy clinical trials of related disorders (27). Primary DAT knockout neurons treated with AAV2.SLC6A3 vector expressed hDAT protein and exhibited dopamine uptake as indicated by reduction of HVA concentration (fig. S13A-D).

AAV2.SLC6A3 was delivered by bilateral stereotactic injection to the substantia nigra (SN) of 4 week old symptomatic knockouts (modelling adolescent patients with DTDS) at 3 dosages: neat = 2×10^{10} , 1;10 = 2×10^9 , 1;100 = 2×10^8 vg/mouse respectively, $n = 8$ per group, 13 males, 11 females from 6 litters). AAV2.GFP control vector was injected to wildtype and knockout littermates (2×10^{10} vg/ mouse, $n = 8$ per group, 7 males, 9 females from 4 litters) (fig. S14A). Growth was equivalent between groups (Fig 7A). Survival was improved in all AAV2.SLC6A3 treated animals compared to AAV2.GFP treated knockouts with 100% survival of the neat dosage group at 12 weeks of age (Fig. 7B). With the lowest dosage (2×10^8 vg/mouse), one mouse developed weight loss and parkinsonism, surviving to P50. Three out of eight (37.5%) AAV2.GFP treated knockouts reached humane endpoint at 5, 6, 8 weeks. At 8 weeks ($n = 5-8$ per group) knockouts treated with highest dosage (2×10^{10} vg/mouse) displayed

motor behavior that was indistinguishable from AAV2.GFP treated wildtypes (Fig. 7C-F, S14B, Supplementary videos 5). Dose response was observed in open field distance travelled and central time (Fig 7C,D S14B, Supplementary video 6). Vertical pole descent time was restored to wildtype times in 2×10^{10} and 2×10^9 vg/mouse but not lowest dosage (2×10^8 vg/mouse) and % foot faults were restored to wildtype rates in all treated knockouts (Fig 7E,F). hDAT staining in midbrain and striatum confirmed midbrain expression with dose-dependent anterograde transport to the striatum (Fig. 7G). Quantification of TH-positive mDA neurons expressing hDAT showed rescue of neurodegeneration (Fig. 7H,I) correlating with midbrain TH transduction, hDAT mRNA transcripts and vector genome copies (vgc) delivered (Fig 7H, S14C-E). Consistent with iPSC-derived mDA, knockouts had significantly lower MAO-A and MAO-B in the midbrain versus wildtype ($P = 0.02$ and 0.001 respectively) (fig. S14F,G). Treatment with AAV2.SLC6A3 neat dosage significantly increased, but did not normalize these enzymes (MAO-A $P = 0.03$ and MAO-B $P = 0.02$) (fig. S14F,G). With targeted stereotactic SN delivery cortical cell loss or vacuolation was not observed (Fig. 7J).

Discussion

Personalized medicine strategies are increasingly important in drug development, particularly for inherited neurodegenerative disorders, where the mainstay of current treatment is symptom control and palliative care. Through the synergistic use of iPSC-derived neuronal and mouse models, we have obtained further insight into the underlying mechanisms governing human disease and have evaluated potential therapeutic strategies for this pharmacoresistant condition. Both models recapitulate important DTDS disease features, with loss of DAT activity, abnormally raised dopamine metabolites and neurodegeneration. The mouse model exhibits key motor features of human patients, with early hyperkinesia evolving into late-stage parkinsonism. Previous studies of DTDS missense variants (which account for 76.6% of DTDS patient mutations) have utilized cell-based overexpression models, *Caenorhabditis elegans* and *Drosophila melanogaster* DAT mutants (3-5,22,23,28). Our iPSC-based platform provides a DTDS model with a number of advantages: it allows the study of patient-relevant DAT mutations in a human derived neuronal model system, including variants that cannot be studied in other models, such as L368Q which confers lethality in the fly model (23). By combining the iPSC and murine disease-relevant models, we have gained further pathophysiological insight into the consequences of loss of DAT function. Both the mDA cell model and knockout murine dissected midbrain show substantial reduction of key enzymes in dopamine catabolism, MAO-A and MAO-B suggesting a compensatory downregulation in the absence of dopamine reuptake. Dysregulation of MAO-A and MOA-B was not evident in patient CSF, however CSF measurement likely does not represent midbrain MAO-A/MAO-B enzyme concentrations. Despite extensive phenotypic rescue of both iPSC and mouse models by gene therapy, restoration of DAT activity did

not fully restore midbrain MAO enzyme concentrations. These studies reflect that MAO regulation is not solely influenced by dopamine reuptake. In the knockout mouse model, we also observed loss of the normal bimodal firing pattern in the medium spiny neuron population, suggesting that DAT deficiency in mDA neurons may have more widespread detrimental systemic effects on synaptic connectivity and post-synaptic neuronal networks.

iPSC-derived mDA neurons and knockouts exhibit neurodegeneration. Although there is limited evidence in patient with DTDS, the progressive nature of clinical disease (4,5,7) and serial DATscan imaging (7) also both point to a neurodegenerative process. From the iPSC-derived mDA model, we postulate that neuronal loss is mediated by an oxidative stress response, secondary to extracellular dopamine toxicity, with proinflammatory cytokine-induced apoptosis. This is corroborated by our findings of raised TNF in CSF of older patients with DTDS with more advanced disease. Overall, it is likely that the mechanisms governing neurodegeneration in DTDS are multifactorial; apoptosis may be driven by factors such as dopamine toxicity and oxidative stress, possibly accelerated by the release of proinflammatory cytokines from activated glia.

Our study highlights the therapeutic limitations of agents such as pifithrin- μ with its mutation-specific chaperone effects (21-23), and in contrast, the wider potential of gene therapy for all patients with DTDS, showing clear evidence of phenotypic rescue in both the cell and knockout mouse model. In the absence of a humanized knock-in mouse, our iPSC-derived model provides potentially clinically-relevant information regarding potential dominant-negative phenomena. Indeed, antagonistic effects from co-expression of both the endogenous mutant allele and wildtype transgene were not observed in the lentivirus-treated cells.

From our study, it is clear that the neuropathological consequences of DTDS are likely to occur early in life. It is universally acknowledged that despite the maturation process, iPSC-derived neurons resemble fetal neurons and indeed the severe cellular phenotype evident in our DTDS mDA cell model suggests prenatal disease onset. The knockout mouse corroborates this, where poor growth and an early progressive motor phenotype with neuronal loss is observed. AAV vectors have been used successfully for clinical translation of targeted intraparenchymal gene therapy in other similar early-onset neurotransmitter disorders (27,29), and hence would be a logical approach to pursue for DTDS, given our highly promising in vivo preclinical data.

We initially sought to explore neonatal gene therapy, given its therapeutic potential for this early onset neurodegenerative disease; the youngest patients benefited most in recent gene therapy clinical trials for Spinal Muscular Atrophy (30) and Mucopolysaccharidosis type IIIa (31). Despite variable gene expression in target mDA neurons, our neonatal gene therapy in knockouts prevented early demise,

1 normalized motor function, restored DAT activity and dopamine homeostasis. Neuronal loss from the
2 SN was prevented, and beneficial effects on the post-synaptic neuronal network included prevention
3 of neuronal loss and normalization of electrophysiological properties of the medium spiny neuron
4 population. Although there was off-target transduction, ectopic overexpression of DAT appeared to
5 be well-tolerated. However, at a ten-fold higher vector dose, we observed off-target neurotoxicity, with
6 astrogliosis in cortical regions and substantial reduction in survival. Neurotoxic effects and reduced
7 survival have been similarly observed in DAT over-expression and ectopic expression transgenic
8 models (32,33). Overall, this strongly suggests that, although low ectopic expression is tolerated, it
9 should ideally be avoided for clinical translatability.

10 The study of Illiano *et al.* provided proof-of-concept for gene therapy of DAT deficiency (34). They
11 delivered two AAV vectors into the midbrain of adult DAT mice by stereotactic injection. To achieve
12 high specificity for dopaminergic neurons, the first AAV expressed Cre recombinase under the control
13 of the truncated rat TH promoter and a second AAV contained murine DAT flanked by loxP sites,
14 under the control of constitutive CMV promoter. Cre recombinase expression thus permitted specific
15 therapeutic DAT expression. Despite this proof-of-concept, such an approach would not be clinically
16 translatable, with the use of murine DAT and potential neurotoxicity of Cre recombinase expression
17 (35).

18 Since both neonatal intracerebroventricular gene delivery (with risk of potential neurotoxic off-target
19 effects) and the dual AAV vector delivery system described above (with neurotoxic Cre recombinase)
20 are unsuitable for clinical translation, we developed a potentially clinically applicable gene therapy
21 approach for patients with DTDS utilizing AAV2 vector, stereotactically targeted to the DAT-expressing
22 SN of the brain. We demonstrated efficacy of the therapeutic expression cassette containing a
23 truncated human promoter and human *SLC6A3* cDNA, in vitro in the patient-derived dopaminergic
24 neuronal cell model, primary knockout neurons and in vivo at different developmental ages of the
25 knockout mouse model. Crucially for clinical translation, we have also demonstrated potential clinical
26 feasibility with a 2 log dose-ranging study of AAV2.SLC6A3 showing clear (dose-dependent)
27 therapeutic efficacy with no evidence of neurotoxicity that might arise from ectopic hDAT expression.

28
29 This study was limited to patient-derived iPSC cell lines and a mouse model in which the mSLC6A3
30 gene was disrupted. Dopaminergic neurotransmission across a functioning synapse was not assessed
31 using this presynaptic iPSC model. However it would be fascinating to do so using organotypic
32 cultures, brain organoids or in vivo optogenetic techniques (36) Some question whether the knockout
33 mouse is a sufficient model for studying cognitive behavioral processes to study neuropsychiatric
34 conditions, prompting the generation of rat models carrying disruptions in the DAT gene (37). It would

1 be interesting to assess therapeutic efficacy of AAV.SLC6A3 on behavioral parameters representing
2 each of the five research domain criteria as previously evaluated in one of these models (38). Although
3 the promising experimental data presented here will advance efforts towards clinical trial, it is important
4 that preclinical studies are repeated in order to obtain long-term readouts, up to a year, of efficacy and
5 to evaluate any evidence of toxicity arising from possible expression of hDAT in non-dopaminergic
6 neurons. Additional challenges relating to human translation are worthy of discussion; for such
7 precision medicine approaches to be effective, there is a need for accurate neurosurgical targeting
8 which requires considerable expertise, and optimal vector dosing to maximise efficacy and avoid
9 neurotoxicity. A clear understanding of the disease is also necessary to ensure that the most suitable
10 patients are put forward for trial, potentially determined by genotype, age and disease stage for
11 optimum therapeutic time window. One potential modification to improve safety and efficacy could be
12 to use a dopaminergic neuron-specific promoter, although the difficulty in identifying a translatable
13 dopaminergic neuron-specific promoter is widely acknowledged in the field. Studies of truncated
14 human TH promoters have shown low to high promoter strength with variable specificity (36). These
15 TH promoters have not been used clinically and unlikely to improve our vector efficacy, safety and
16 translatability. Moreover, the current gene therapy trials for related disorders such as AADC deficiency:
17 (NCT01395641, NCT01973543) utilize the AAV2 capsid with a ubiquitous promoter, combined with
18 stereotactic delivery to successfully target specific brain regions such as the striatum and midbrain
19 with striking patient benefit (39-41). Our use of hSyn promoter improves neuronal selectivity in
20 comparison and the efficacy and safety achieved through our vector design and delivery method
21 clearly supports future translation of our approach towards a clinical trial of AAV gene therapy for
22 patients with DTDS.

24 **Material and Methods**

25 **Study design**

26 The aim of this study was to (i) understand the mechanisms underpinning DTDS in an in vitro patient-
27 derived midbrain dopaminergic (mDA) model, and (ii) develop a gene therapy strategy to rescue
28 disease in vitro and in vivo.

29 For the generation of a patient-derived neuronal model, we obtained fibroblasts from patients and
30 reprogrammed them into iPSCs. In order to rule out effect genetic background, we generated an
31 isogenic control iPSC line with correction of the disease-associated homozygous *SLC6A3* mutation.
32 A tritiated dopamine uptake assay and High Performance Liquid Chromatography (HPLC) were
33 performed to confirm DAT dysfunction in mature derived mDA neurons. We then investigated cellular

disease mechanisms by immunoblotting, qRT-PCR and immunofluorescence analysis, identifying disease-specific dysregulation of DA metabolites and neurodegenerative processes. A cell viability assay was performed on the mDA cultures to investigate inflammatory response and an ELISA assay on patient CSF to investigate pro-inflammatory cytokine release. We then developed a lentiviral-based gene therapy delivery approach and analyzed DAT activity and markers of neurodegeneration, post-gene transfer.

For reproducibility and reliability of our dataset, we have used standardized protocols and performed blinded analyses, except in Fig. 3D, 5D and S2B. The number of replications of each independent experiment is reported in the respective figure legends. Single experiments, which failed for technical reasons, have been selectively discarded from the analysis. Tritiated dopamine uptake assays of untreated (Fig. 1A) and pifithrin- μ treated (Fig. 5A) lines have been performed simultaneously to avoid technical variability and as such, they partially share the same dataset for untreated samples.

The in vivo studies were designed to test the hypothesis that AAV-mediated gene therapy would restore DAT function in DAT-KO mouse model of DTDS. We evaluated the efficacy of neonatal AAV9 mediated gene transfer with endpoints of survival, locomotor behavior and neurotransmitter analysis. We assessed toxicity related to dosage and off-target expression and then delivered gene therapy to adult DAT-KO mice with AAV2 capsid by stereotactic injection with the same endpoints. The number of biological replicates varied between studies ($n = 5-17$) and is indicated in the figure legends. Animals were randomly assigned to the vector treatment group. Assessment of outcomes was blinded through labelling without treatment information on behavioral analysis videos, tissue samples for biodistribution and pathological analysis.

Statistical Analysis

Statistical analysis tailored to each experiment was performed using GraphPad Prism version 8. For the statistical analysis of iPSCs derived data, when dual comparisons were required two-tailed Student's t-test was applied, whereas for multiple comparisons one-way analysis of variance (ANOVA) was performed. In vivo experimental design and sample sizes were designed using NC3Rs guidance and power calculation. For most analyses of animal experiments, one-way or two-way ANOVA was performed with either Bonferroni or Tukey's multiple comparison. % foot faults were converted by log transformation before ANOVA. For neuronal firing Kruskal-Wallis distribution and χ^2 tests were applied.

Supplementary Materials

Supplementary Methods

Supplementary Figure 1: Generation of control, patient and isogenic iPSC lines

Supplementary Figure 2: Differentiation of control and patient iPSC lines into midbrain dopaminergic precursors

Supplementary Figure 3: Differentiation of control and patient neural progenitors into mature, electrically active mDA neurons

Supplementary Figure 4: d65 DAT gene and protein expression profiles for control and patient lines

Supplementary Figure 5: d65 gene expression profiles for key enzymes involved in dopamine metabolism in control and patient lines

Supplementary Figure 6: d65 quantification of mDA neurons in control and patient lines

Supplementary Figure 7: d65 immunofluorescence for cleaved caspase-3 (cCASP3) in control and patient lines

Supplementary Figure 8: d65 immunofluorescence for GFAP in control and patient lines

Supplementary Figure 9: Therapeutic approaches for DTDS with pifithrin- μ and lentiviral gene transfer in the mDA neuronal model

Supplementary Figure 10: In vivo AAV9 hSyn GFP marker gene study

Supplementary Figure 11: Electrophysiological properties of Medium Spiny Neurons following neonatal AAV9 hSLC6A3 gene therapy

Supplementary Figure 12: AAV9.hSLC6A3 intracerebroventricular gene transfer at higher dosage

Supplementary Figure 13: AAV2.hSLC6A3 in vitro transduction of knockout primary neurons

Supplementary Figure 14: AAV2.hSLC6A3 stereotactic gene delivery to substantia nigra

Supplementary Table 1: Primers for CRISPR correction of *SLC6A3* variant c.1184C>T

Supplementary Table 2: List of antibodies

Supplementary Table 3: Primers sequences

Supplementary Table 4: Primers sequences for generation of vector expression cassette, viral vector titration and qRT-PCR

movie 1: Untreated hyperlocomotor DAT knockout at P21

Supplementary movie 2: Untreated DAT knockout showing parkinsonism at P35

Supplementary movie 3: Open field DAT knockout treated with AAV9.hSLC6A3

Supplementary movie 4: Open field DAT knockout treated with high dosage AAV9.hSLC6A3

Supplementary movie 5: Open field DAT knockout treated with neat AAV2.hSLC6A3 compared with controls.

Supplementary movie 6: Open field dosage response of DAT knockout treated with AAV2.SLC6A3 2×10^{10} (neat), 2×10^9 (1:10), 2×10^8 (1:100) dosages

1 Data file S1: Raw data (provided as separate Excel file)

2

3 References

- 4 1. W. Poewe, K. Seppi, C. M. Tanner, G. M. Halliday, P. Brundin, J. Volkmann, A. E. Schrag, A.
5 E. Lang, Parkinson disease, *Nature Reviews. Disease primers* **3**, 17013 (2017).
- 6 2. G. Massaro, C. N. Z. Mattar, A. M. S. Wong, E. Sirka, S. M. K. Buckley, B. R. Herbert, S.
7 Karlsson, D. P. Perocheau, D. Burke, S. Heales, A. Richard-Londt, S. Brandner, M. Huebecker, D. A.
8 Priestman, F. M. Platt, K. Mills, A. Biswas, J. D. Cooper, J. K. Y. Chan, S. H. Cheng, S. N. Waddington,
9 A. A. Rahim, Fetal gene therapy for neurodegenerative disease of infants. *Nature Medicine* **24**, 1317-
10 1323 (2018).
- 11 3. M. A. Kurian, J. Zhen, S. Y. Cheng, Y. Li, S. R. Mordekar, P. Jardine, N. V. Morgan, E. Meyer,
12 L. Tee, S. Pasha, E. Wassmer, S. J. Heales, P. Gissen, M. E. Reith, E. R. Maher, Homozygous loss-
13 of-function mutations in the gene encoding the dopamine transporter are associated with infantile
14 parkinsonism-dystonia. *The Journal of Clinical Investigation* **119**, 1595-1603 (2009).
- 15 4. M. A. Kurian, Y. Li, J. Zhen, E. Meyer, N. Hai, H. J. Christen, G. F. Hoffmann, P. Jardine, A.
16 von Moers, S. R. Mordekar, F. O'Callaghan, E. Wassmer, E. Wraige, C. Dietrich, T. Lewis, K. Hyland,
17 S. Heales, Jr., T. Sanger, P. Gissen, B. E. Assmann, M. E. Reith, E. R. Maher, Clinical and molecular
18 characterisation of hereditary dopamine transporter deficiency syndrome: an observational cohort and
19 experimental study. *The Lancet Neurology* **10**, 54-62 (2011).
- 20 5. J. Ng, J. Zhen, E. Meyer, K. Erreger, Y. Li, N. Kakar, J. Ahmad, H. Thiele, C. Kubisch, N. L.
21 Rider, D. H. Morton, K. A. Strauss, E. G. Puffenberger, D. D'Agnano, Y. Anikster, C. Carducci, K.
22 Hyland, M. Rotstein, V. Leuzzi, G. Borck, M. E. Reith, M. A. Kurian, Dopamine transporter deficiency
23 syndrome: phenotypic spectrum from infancy to adulthood. *Brain* **137**, 1107-1119 (2014).
- 24 6. G. E. Torres, R. R. Gainetdinov, M. G. Caron, Plasma membrane monoamine transporters:
25 structure, regulation and function. *Nature Reviews Neuroscience* **4**, 13-25 (2003).
- 26 7. F.H. Hansen, T. Skjørringe, S. Yasmeen, N.V. Arends, M.A. Sahai, K. Erreger, T.F.
27 Andreassen, M. Holy, P.J. Hamilton, V. Neergheen, M. Karlsborg, A.H. Newman, S. Pope, S.J.
28 Heales, L. Friberg, I. Law, L.H. Pinborg, H.H. Sitte, C. Loland, L. Shi, H. Weinstein, A. Galli, L.E.

- 1 Hjermind, L.B. Møller, U. Gether, Missense dopamine transporter mutations associate with adult
2 parkinsonism and ADHD. *The Journal of Clinical Investigation* **124**, 3107-3120 (2014).
- 3 8. Y. Yildiz, E. Pektas, A.Tokatli, G. Haliloglu, Hereditary Dopamine Transporter Deficiency
4 Syndrome: Challenges in Diagnosis and Treatment. *Neuropaediatrics* **48**, 49-52(2017).
5
- 6 9. A. Kuster, J.B Arnoux, M. Barth, D. Lamireau, N. Houcinat, C. Goizet, B. Doray, S. Gobin, M.
7 Schiff, A. Cano, D. Amsallem, C. Barnerias, B. Chaumette, M. Plaze, A. Slama. C. loos. I.Desguerre,
8 A.S.Lebre, P. de Lonlay, L.Christa, Diagnostic approach to neurotransmitter monoamine disorders:
9 experience from clinical, biochemical, and genetic profiles. *Journal of Inherited Metabolic Disorders*
10 **41**,129-139 (2018).
11
- 12 10. A. Galiart, P.Weber, A.N. Datta. Infantile Dystonia Parkinsonism caused by mutations in
13 SLC6A3: Case report of three siblings, *Neuropediatrics* **48**:S1-S45 (2017).
14
- 15 11. E. Heidari, E.Razmara, S.Hosseinpour, A. R.Tavasoli, M.Garshasbi, Homozygous in-frame
16 variant of SCL6A3 causes dopamine transporter deficiency syndrome in a consanguineous family.
17 *Annals of Human Genetics*, **84**, 315-323 (2020).
- 18 12. M. Baga, C. Spagnoli C, L Soliano, G.G. Salerno, S. Rizzi, D. Frattini, F. Pisani, C. Fusco,
19 Early-onset Dopamine Transporter Deficiency Syndrome: Long-term Follow-up. *Can J Neurol Sci* **1**,
20 1-2. (2020) doi: 10.1017/cjn.2020.144.
21
- 22 13. M.M. Nasehi, A. Nikkah, M. Salari, P. Soltani, S. Shirzadi. Dopamine Transporter Deficiency
23 Syndrome: a case with hyper and hypokinetic extremes. *Movement Disorders Clinical Practice* **7**
24 S3,57-60 (2020).
25
- 26 14. A. Kirkeby, S. Grealish, D. A. Wolf, J. Nelander, J. Wood, M. Lundblad, O. Lindvall, M. Parmar,
27 Generation of regionally specified neural progenitors and functional neurons from human embryonic
28 stem cells under defined conditions, *Cell Reports* **1**, 703-714 (2012).
- 29 15. D. Lehnen, S. Barral, T. Cardoso, S. Grealish, A. Heuer, A. Smiyakin, A. Kirkeby, J. Kollet, H.
30 Cremer, M. Parmar, A. Bosio, S. Knobel, IAP-Based Cell Sorting Results in Homogeneous
31 Transplantable Dopaminergic Precursor Cells Derived from Human Pluripotent Stem Cells. *Stem Cell*
32 *Reports* **9**, 1207-1220 (2017).

- 1 16. R. M. Ransohoff, How neuroinflammation contributes to neurodegeneration. *Science* **353**,
2 777-783 (2016).
- 3 17. M. Sochocka, B. S. Diniz, J. Leszek, Inflammatory Response in the CNS: Friend or Foe?
4 *Molecular Neurobiology* **54**, 8071-8089 (2017).
- 5 18. Q. He, Q. Wang, C. Yuan, Y. Wang, Downregulation of miR-7116-5p in microglia by MPP(+)
6 sensitizes TNF-alpha production to induce dopaminergic neuron damage. *Glia* **65**, 1251-1263 (2017).
- 7 19. V. Sanchez-Guajardo, N. Tentillier, M. Romero-Ramos, The relation between alpha-synuclein
8 and microglia in Parkinson's disease: Recent developments. *Neuroscience* **302**, 47-58 (2015).
- 9 20. K. Hyland, R.A. Surtees, S.J. Heales, A.Bowron, D.W.Howells, I.Smith, Cerebrospinal fluid
10 concentrations of pterins and metabolites of serotonin and dopamine in a pediatric reference
11 population. *Pediatr Res.* **1**;10-14 (1993).
- 12 21. A. Kasture, A. El-Kasaby, D. Szollosi, H. M. M. Asjad, A. Grimm, T. Stockner, T. Hummel, M.
13 Freissmuth, S. Sucic, Functional Rescue of a Misfolded *Drosophila melanogaster* Dopamine
14 Transporter Mutant Associated with a Sleepless Phenotype by Pharmacological Chaperones. *The*
15 *Journal of Biological Chemistry* **291**, 20876-20890 (2016).
- 16 22. P. Beerepoot, V. M. Lam, A. Salahpour, Pharmacological Chaperones of the Dopamine
17 Transporter Rescue Dopamine Transporter Deficiency Syndrome Mutations in Heterologous Cells.
18 *The Journal of Biological Chemistry* **291**, 22053-22062 (2016).
- 19 23. H. M. M. Asjad, A. Kasture, A. El-Kasaby, M. Sackel, T. Hummel, M. Freissmuth, S. Sucic,
20 Pharmacochaperoning in a *Drosophila* model system rescues human dopamine transporter variants
21 associated with infantile/juvenile parkinsonism. *The Journal of Biological Chemistry* **292**, 19250-
22 19265 (2017).
- 23 24. B. Giros, M. Jaber, S. R. Jones, R. M. Wightman, M. G. Caron, Hyperlocomotion and
24 indifference to cocaine and amphetamine in mice lacking the dopamine transporter. *Nature* **379**, 606-
25 612 (1996).
- 26 25. M. Cyr, J. M. Beaulieu, A. Laakso, T. D. Sotnikova, W. D. Yao, L. M. Bohn, R. R. Gainetdinov,
27 M. G. Caron, Sustained elevation of extracellular dopamine causes motor dysfunction and selective
28 degeneration of striatal GABAergic neurons. *Proceedings of the National Academy of Sciences of the*
29 *United States of America* **100**, 11035-11040 (2003).

26. G. Murlidharan, R.J Samulski, Aravind Asokan, Biology of adeno-associated viral vectors in the central nervous system. *Front Mol Neurosci.* **7**, 76 (2014)
27. W. L. Hwu, S. Muramatsu, S. H. Tseng, K. Y. Tzen, N. C. Lee, Y. H. Chien, R. O. Snyder, B. J. Byrne, C. H. Tai, R. M. Wu, Gene therapy for aromatic L-amino acid decarboxylase deficiency. *Science Translational Medicine* **4**, 134ra161 (2012).
28. P. Illiano, A. Lanzo, D. Leo, M. Paglione, G. Zampi, R.R. Gainetdinov, E. Di Schiavi, A. Caenorhabditis elegans model to study dopamine transporter deficiency syndrome. *European Journal of Neuroscience* **45**, 207-214 (2017).
29. Y.H. Chien, N.C. Lee, S.H. Tseng, C.H. Tai, S. Muramatsu, B.J. Byrne, W.L. Hwu. Efficacy and safety of AAV2 gene therapy in children with aromatic L-amino acid decarboxylase deficiency: an open-label, phase 1/2 trial, *Lancet Child & Adolescent Health* **1**, 265-273 (2017).
30. J. R. Mendell, S. Al-Zaidy, R. Shell, W. D. Arnold, L. R. Rodino-Klapac, T. W. Prior, L. Lowes, L. Alfano, K. Berry, K. Church, J. T. Kissel, S. Nagendran, J. L'Italien, D. M. Sproule, C. Wells, J. A. Cardenas, M. D. Heitzer, A. Kaspar, S. Corcoran, L. Braun, S. Likhite, C. Miranda, K. Meyer, K. D. Foust, A. H. M. Burghes, B. K. Kaspar, Single-Dose Gene-Replacement Therapy for Spinal Muscular Atrophy. *The New England Journal of Medicine* **377**, 1713-1722 (2017).
31. M. Tardieu, M. Zerah, B. Husson, S. de Bournonville, K. Deiva, C. Adamsbaum, F. Vincent, M. Hocquemiller, C. Broissand, V. Furlan, A. Ballabio, A. Fraldi, R. G. Crystal, T. Baugnon, T. Roujeau, J. M. Heard, O. Danos, Intracerebral administration of adeno-associated viral vector serotype rh.10 carrying human SGSH and SUMF1 cDNAs in children with mucopolysaccharidosis type IIIA disease: results of a phase I/II trial. *Human Gene Therapy* **25**, 506-516 (2014).
32. S.T. Masoud, L.M. Vecchio, Y. Bergeron, M.M. Hossain, L.T. Nguyen, M.K. Bermejo, B. Kile, T.D. Sotnikova, W.B. Siesser, R.R. Gainetdinov, R.M. Wightman, M.G. Caron, J.R. Richardson, G.W. Miller, A.J. Ramsey, M. Cyr, A. Salahpour, Increased expression of the dopamine transporter leads to loss of dopamine neurons, oxidative stress and L-DOPA reversible motor deficits. *Neurobiological Diseases* **74**:66-75 (2015).

33. L. Chen, Y. Ding, B. Cagniard, A.D. Van Laar, A. Mortimer, T. Chi, T.G. Hastings, U.J. Kang, X. Zhuang, Unregulated cytosolic dopamine causes neurodegeneration associated with oxidative stress in mice. *Journal of Neuroscience* **28**, 425-433 (2008).
34. P.Illiano, C.E.Bass, L.Fichera, L.Mus, E.A.Budygin, T.D.Sitnikova, D.Leo. S.Espinoza, R.R. Gainetdinov, Recombinant Adeno-Associated Virus-mediated rescue of function in a mouse model of Dopamine Transporter Deficiency Syndrome. *Scientific Reports* **4**, 46280 (2017).
35. A.S. Rezai, C Gruszczynski, B.P.Guiard, J.M Launay, F Louis, C.Betancor, V. Vialou, S. Gautron, Viral vector-mediated Cre recombinase expression in substantia nigra induces lesions of the nigrostriatal pathway associated with perturbations of dopamine-related behaviors and hallmarks of programmed cell death. *Journal of Neurochemistry* **3**, 330-340 (2019).
36. C. Liu, L. Kershberg , J. Wang, S. Schneeberger, P.S. Kaeser. Dopamine Secretion Is Mediated by Sparse Active Zone-like Release Sites. *Cell* **172**, 706-18.e15 (2018).
37. D. Leo, I. Sukhanov, F. Zoratto, P. Illiano, L. Caffino, F. Sanna, G. Messa, M. Emanuele, A. Esposito, M. Dorofeikova, E.A. Budygin, L. Mus, E.V. Efimova , M. Niello, S. Espinoza, T.D. Sotnikova, M.C. Hoener, G. Laviola, F. Fumagalli, W, Adriani, R.R. Gainetdinov. Pronounced Hyperactivity, Cognitive Dysfunctions, and BDNF Dysregulation in Dopamine Transporter Knock-out Rats. *J Neurosci.* **38**,1959-72 (2018).
38. V. Vengeliene, A. Bespalov, M, Rossmanith, S. Horschitz, S. Berger, A.L. Relo, H.R. Noori, P. Schneider, T. Enkel, D. Bartsch, M. Schneider, B. Behl, A.C. Hansson, P. Schloss, R. Spanagel. Towards trans-diagnostic mechanisms in psychiatry: neurobehavioral profile of rats with a loss-of-function point mutation in the dopamine transporter gene. *Dis Model Mech* **10**, 451-61 (2017).
39. A.S. Rolland, T. Kareva, O Yarygina, N. Kholodilov, R.E. Burke. Expression mediated by three partial sequences of the human tyrosine hydroxylase promoter *in vivo*. *Molecular Therapy Methods & Clinical Development* **2**, 16062 (2016).
40. C.W. Christine, K.S. Bankiewicz, A.D. Van Laar, R.M. Richardson, B. Ravina, A.B. Kells, B. Boot, A.J. Martin, J. Nutt, M.E. Thompson, P.S. Larson, Magnetic resonance imaging-guided phase

1 1 trial of putaminal AADC gene therapy for Parkinson's disease. *Annals of Neurology* **5**, 704-
2 714(2019).

3 41. S. Palfi, J. M. Gurruchaga, G. S. Ralph, H. Lepetit, S. Lavis, P. C. Buttery, C. Watts, J.
4 Miskin, M. Kelleher, S. Deeley, H. Iwamuro, J. P. Lefaucheur, C. Thiriez, G. Fenelon, C. Lucas, P.
5 Brugieres, I. Gabriel, K. Abhay, X. Drouot, N. Tani, A. Kas, B. Ghaleh, P. Le Corvoisier, P. Dolphin,
6 D. P. Breen, S. Mason, N. V. Guzman, N. D. Mazarakis, P. A. Radcliffe, R. Harrop, S. M. Kingsman,
7 O. Rascol, S. Naylor, R. A. Barker, P. Hantraye, P. Remy, P. Cesaro, K. A. Mitrophanous, Long-term
8 safety and tolerability of ProSavin, a lentiviral vector-based gene therapy for Parkinson's disease: a
9 dose escalation, open-label, phase 1/2 trial. *Lancet* **383**, 1138-1146 (2014).

10 42. W. San Sebastian, A.P. Kells, J. Bringas, L. Samaranch, P. Hadaczek, A. Ciesielska,
11 M. Macavan, P.J. Pivrotto, J. Forsayeth, S. Osborne, J.F. Wright, F. Green, G. Heller, K.S. Bankiewicz.
12 Safety and tolerability of MRI-guided infusion of AAV2-AADC into the midbrain of non-human primate.
13 *Molecular Therapy Methods & Clinical Development* **3**, 14049 (2014).

14 43. M. Lenz, R. Goetzke, A. Schenk, C. Schubert, J. Veeck, H. Hemeda, S. Koschmieder, M.
15 Zenke, A. Schuppert, W. Wagner, Epigenetic Biomarker to Support Classification into Pluripotent and
16 Non-Pluripotent Cells. *Scientific Reports* **5**, 8973 (2015).

17 44. M. E. Reith, C. Xu, F. I. Carroll, N. H. Chen, Inhibition of [3H]dopamine translocation and
18 [3H]cocaine analog binding: a potential screening device for cocaine antagonists. *Methods in*
19 *Enzymology* **296**, 248-259 (1998).

20 45. C. de la Fuente, D. G. Burke, S. Eaton, S. J. R. Heales, Inhibition of neuronal mitochondrial
21 complex I or lysosomal glucocerebrosidase is associated with increased dopamine and serotonin
22 turnover. *Neurochemistry International* **109**, 94-100 (2017).

23 46. S. Kugler, E. Kilic, M. Bahr, Human synapsin 1 gene promoter confers highly neuron-specific
24 long-term transgene expression from an adenoviral vector in the adult rat brain depending on the
25 transduced area. *Gene Therapy* **10**, 337-347 (2003).

26 47. T. Dull, R. Zufferey, M. Kelly, R. J. Mandel, M. Nguyen, D. Trono, L. Naldini, A third-generation
27 lentivirus vector with a conditional packaging system. *Journal of Virology* **72**, 8463-8471 (1998).

28 48. S. Charrier, M. Ferrand, M. Zerbato, G. Precigout, A. Viorner, S. Bucher-Laurent, S. Ziyat
29 Benkhelifa, O.W. Merten, J. Perea, A. Galy, Quantification of lentiviral vector copy numbers in individual

hematopoietic colony-forming cells shows vector dose-dependent effects on the frequency and level of transduction. *Gene Therapy* **5**, 479-87 (2011).

49. C.J. Binny, A.C.Nathwani, Vector systems for prenatal gene therapy: principles of adeno-associated virus vector design and production. *Methods Molecular Biology* 891:109–131(2012).

50. J. Y. Kim, S. D. Grunke, Y. Levites, T. E. Golde, J. L. Jankowsky, Intracerebroventricular viral injection of the neonatal mouse brain for persistent and widespread neuronal transduction. *Journal of visualized experiments : JoVE*, **71** 51863 (2014).

51. G. Paxinos, K. F. Paxinos and Franklin's the Mouse Brain in Stereotaxic Coordinates. São Paulo, Academic Press 360 p. <https://www.elsevier.com/books/paxinos-and-franklins-the-mouse-brain-in-stereotaxic-coordinates/paxinos/978-0-12-391057-8> (2012).

52. A. A. Rahim, A. M. Wong, K. Hoefer, S. M. Buckley, C. N. Mattar, S. H. Cheng, J. K. Chan, J. D. Cooper, S. N. Waddington, Intravenous administration of AAV2/9 to the fetal and neonatal mouse leads to differential targeting of CNS cell types and extensive transduction of the nervous system. *FASEB journal : official publication of the Federation of American Societies for Experimental Biology* **25**, 3505-3518 (2011).

Acknowledgments: We sincerely thank our patients and their families for participating in this study. We thank UCL Genomics (UCL GOS-Institute of Child Health) for undertaking SNP microarray studies. This research was supported by the NIHR Great Ormond Street Hospital Biomedical Research Centre. The views expressed are those of the author(s) and not necessarily those of the NHS, the NIHR or the Department of Health. We thank GOS-Institute of Child Health Biomedical Research Centre for support in statistical analysis and the MRC Centre for Neuromuscular Disorders Biobank for providing age-matched control fibroblasts. We thank Professors Vincenzo Leuzzi and Bruria Ben Zeev for providing patient fibroblasts and Drs Hugo Sampaio, Sushil Bandodkar, Rafa Artuch and Ann Agnes Mathew for providing patient CSF towards this study. We thank Professors Marc G Caron, Raul R Gainetdinov and Ms Wendy Roberts for support with the mouse transgenic colony. We thank Lorita Gianfrancesco for proof-reading the manuscript.

Funding: This research was supported through Wellcome Intermediate Clinical Fellowship (WT098524MA to M.A.K. and S.B.), UK Medical Research Council (MRC) Clinical Research training fellowship (MR/K02342X/1 to J.N.), MRC Biomedical Catalyst Developmental Pathway Funding

Scheme (MR/R015325/1 to S.N.W, M.A.K, A.A.R, J.N.), Great Ormond Street Hospital Children's Charity and the Rosetrees Trust, Robert Luff Foundation and John Black Foundation (V1284 and M576 to M.A.K., J.N, S.N.W.), NIHR Research Professorship (NIHR-RP-2016-07-019 to M.A.K) and Sir Jules Thorn Award for Biomedical Research (M.A.K).

Marie Skłodowska-Curie Actions of the European Union's Seventh Framework Programme FP7 under REA grant agreement for "Training in Neurodegeneration, Therapeutics, Intervention and Neurorepair" (608381 to CDLFB); Epilepsy Research UK F1701 Marie-Cure Fellowship 658418 to G.L.). Joan Pitts-Tucker/Moritz studentship (to R.W.); UCL IMPACT PhD studentship (to R.P); H.A. is funded by Kuwait University. The Monument Trust Discovery Award from Parkinson's UK (Grant J-1403 to R.W-M, J.V. and S.A.C.); the National Institute for Health Research (544454 to G.R.); MRC, Sparks, LifeArc and Great Ormond Street Children's Charity & Dravet Syndrome UK (MR/P026494/1, 17UCL01, P2020-0008 and V4720 to R.K. St.S. and S.N.W); MRC (MR/N019075/1 to D.P. and J.B.); Action Medical Research for Children Charity Nutricia Metabolic Research Grant (GN2137 to J.B.); London Advanced Therapy/Confidence in Collaboration (2CiC017, MRC MR/T008024/1 to J.B); Wellbeing of Women fellowship (RT-414 to N.S.); CONICYT Becas Chile Doctoral Fellowship Program (72160294 to J.A.D.) and LifeArc (P2020-0008 to J.A.D); the Royal Society (UF140596 to St.S.); Versus Arthritis (PhD scholarship 21552 and grant 21593 to L.R.M.); Austrian Science Fund FWF (P31255-B27 to S.S) and SFB35-10, LSC17-026 to M.F.); Wellcome Innovator Award (21077/Z/18/Z to J.R.C.); Muscular Dystrophy UK and Association Française contre les myopathies (Translasmuscle program, project 19507 and 22946 to M.B.). MRC (MR/N026101/1 to A.A.R. and S.N.W., and MR/R025134/1, MR/S009434/1, MR/S036784/1, MR/T044853/1 to A.A.R.), NC3Rs (NC/L001780/1 to A.A.R. and S.N.W.); Wellcome Trust Institutional Strategic Support Fund/UCL Therapeutic Acceleration Support (TAS) Fund (204841/Z/16/Z to A.A.R.), European Union's Horizon 2020 research and innovation program under grant agreement no. 666918 (BATCure to A.A.R.), Action Medical Research (GN2485 to A.A.R). A.A.R is supported from UK Gauchers Association, and Asociación Niemann Pick de Fuenlabrada and NIHR GOSH BRC (the views expressed are those of the author(s) and not necessarily those of the NHS, the NIHR or the Department of Health).

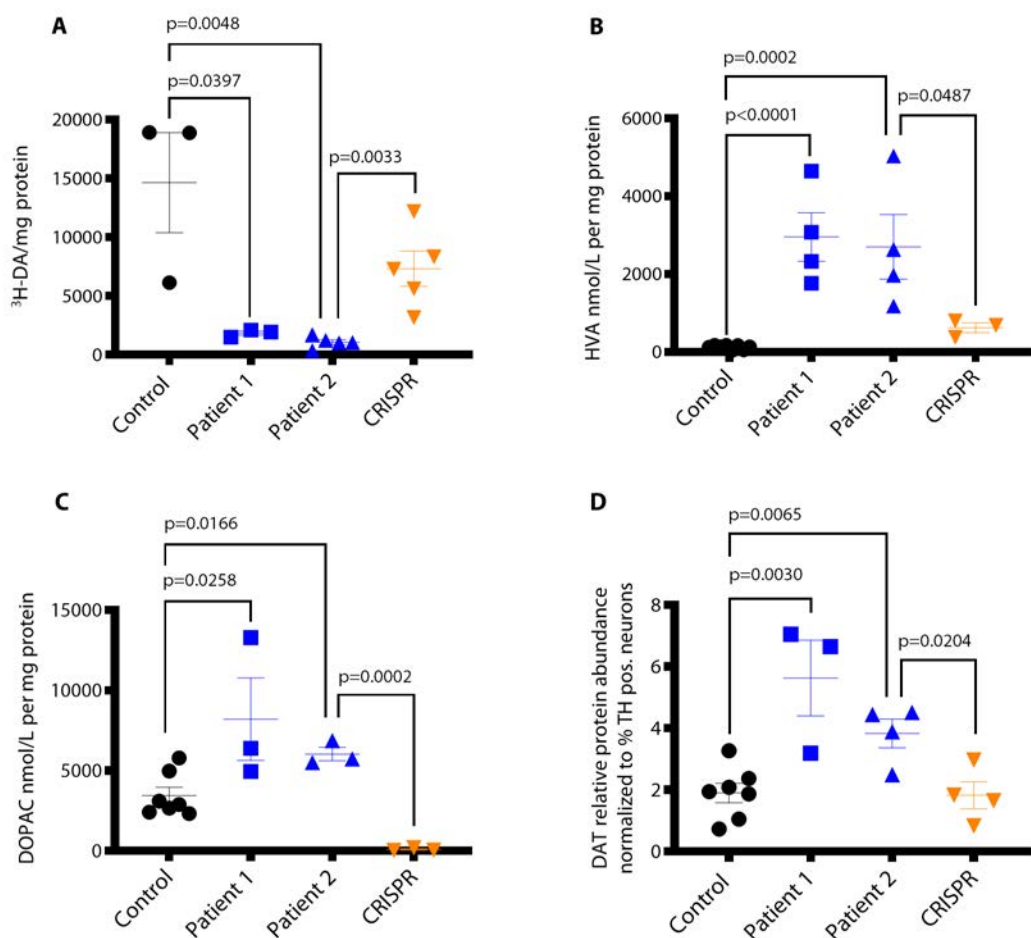
Author Contributions: M.A.K. conceived and designed the study. S.N.W. designed the study. J.N. designed and performed experiments and data analysis for the in vivo study. S.B. designed and performed experiments and data analysis for the in vitro study. C.D.L.F.B and H.A. performed HPLC analysis, supervised by S.P. and S.J.R.H. G.L. and St.S. performed patch clamp electrophysiology and analysis. F.A.E., G.R. and S.H. contributed to in vitro experiments. R.W. performed tritiated dopamine uptake analysis, supervised by R.W-M. J.N., J.R.C., R.P., R.K., D.P., J.B., N.J.S., J.A.D., A.A.R. and S.N.W. contributed to gene therapy construct design, vector production, in vivo experiments and analysis. E.M. and A.N. performed Sanger sequencing and data analysis. J.N.,

1 S.N.W., S.B. and M.B. performed the teratoma test. J.V. and S.A.C. contributed to iPSC generation.
2 L.R.M performed cytometric bead assay. So.S. and M.F. provided pifithrin- μ . M.B. designed and
3 performed the cytotoxicity assay and undertook data analysis. J.N., S.B., S.N.W. and M.A.K. drafted
4 the manuscript and F.A.E, R.W., C.D.L.F.B, G.L., A.N. and M.B. contributed to written sections of the
5 manuscript. St.S, S.A.C., M.F., S.J.R.H, R.W-M. and M.B., provided input for manuscript revision. All
6 authors reviewed the manuscript prior to submission.

7
8
9 **Competing interest:** M.A.K. was sponsored by Agilis to attend AADC Deficiency International
10 Advisory Board (AADC-D IAB) - June 27th 2018. SNW has previous or existing consultancy
11 agreements with ONO Pharmaceuticals, Synpromics Ltd., Reliance Biosciences, Codiak Biosciences,
12 Takeda Pharmaceutical Company, LivaNova Plc. Consultancy agreements with Biormarin (M.A.K,
13 S.N.W) and Albion Capital (S.N.W., J.N.). S.N.W and J.N hold sponsored research agreements with
14 Rocket Pharma and Synpromics Ltd.

15
16 **Data and materials availability:** All data associated with study are available in main text or the
17 Supplementary Materials.

1 Figure Legends



2

3 Figure 1: DTDS-patient derived mDA neurons recapitulate key disease features

4 **A** [^3H]dopamine uptake measured at d65. Values are relative to protein concentration (n = 3, 3, 5, 5
5 for Control, Patient 1, Patient 2 and CRISPR, respectively). **B, C** HPLC detection of extracellular HVA
6 and DOPAC at d65 (n = 8, 4, 4, 3 respectively, and n = 7, 3, 3, 3 respectively). **D** Quantification of
7 DAT protein detected in d65 neurons derived from Control, Patient 1, Patient 2 and CRISPR lines,
8 relative to GAPDH, and normalized to percentage of TH positive cells in each neuronal population as
9 reported in Fig.3B (n = 7, 3, 4 and 4 respectively). Error bars indicate SEM. Both DTDS lines were
10 independently compared to controls using two-tailed Student's *t*-test for all analyses.

11

12

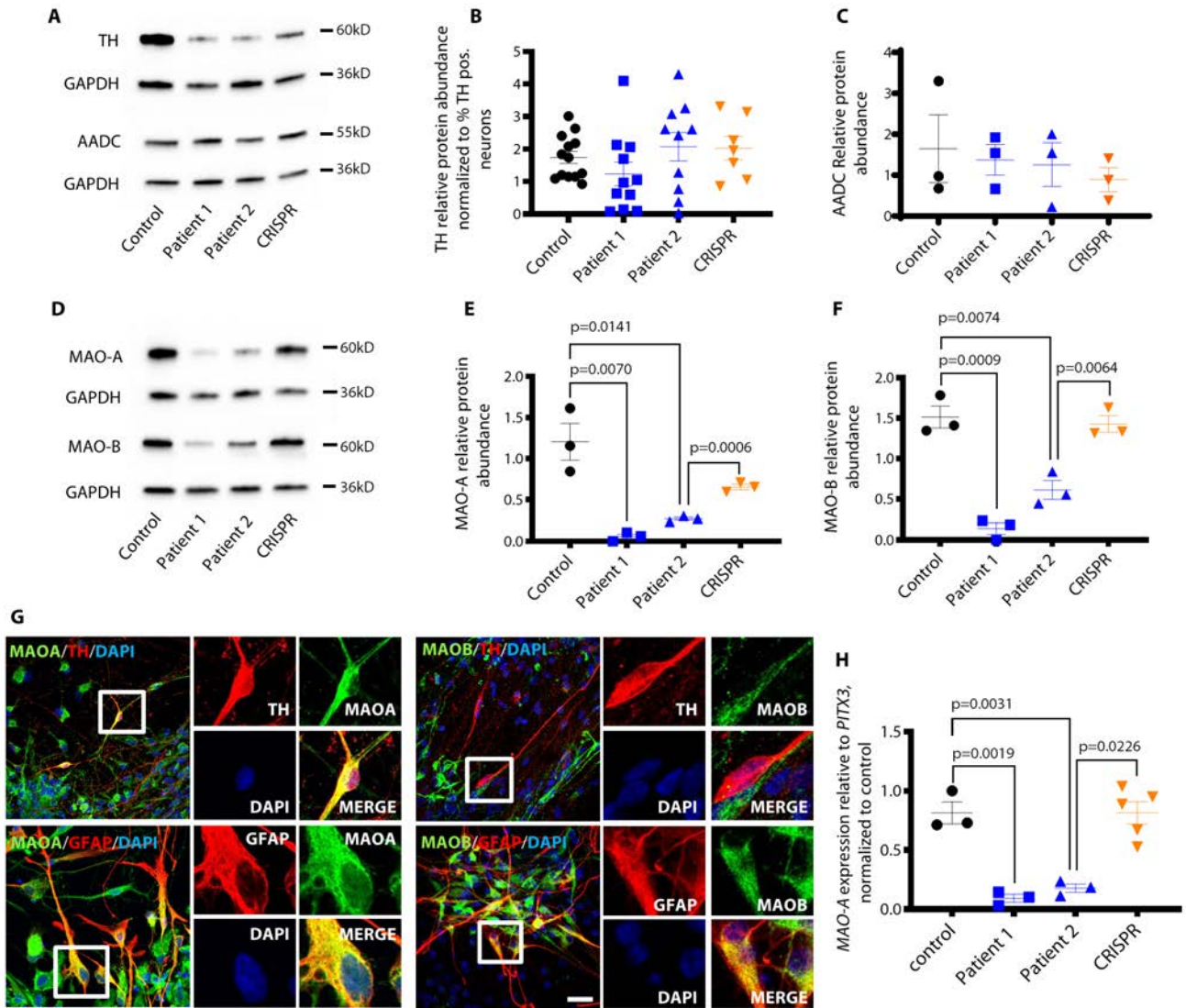


Figure 2: DTDS-patient derived mDA neurons show dysregulation of key enzymes involved in dopamine catabolism

A Cropped immunoblot of total TH protein and AADC detected at d65. **B** Relative abundance of TH protein detected at d65 in Control, Patient 1, Patient 2 and CRISPR, relative to housekeeping gene GAPDH and normalized to percentage of TH positive cells in each sample as reported in Fig. 3B (n = 13, 11, 10, 7 respectively). **C** Quantification of AADC protein relative to GAPDH (n = 3 per line). **D** Cropped immunoblot of total MAO-A, MAO-B and GAPDH at d65. **E** Quantification of MAO-A protein relative to GAPDH (n = 3 per line). **F** Quantification of relative MAO-B abundance in control and patient-derived neurons (n = 3 per line). **G** Immunofluorescence analysis of MAO-A/TH and MAO-A/GFAP (left panel) and MAO-B/TH and MAO-B/GFAP (right panel) in Control mDA neural culture at day 65 of differentiation. Nuclei were counterstained with DAPI (blue). Scale bar 20μm. **H** qRT-PCR for MAO-A at d65 in Control, Patient 1, Patient 2 and CRISPR. mRNA values are relative to the

- 1 midbrain dopaminergic related gene *PITX3* and normalized to control (n = 3, 3, 3, 5 respectively).
- 2 Error bars indicate SEM. Both DTDS lines were independently compared to controls using two-tailed
- 3 Student's *t*-test for all analyses.

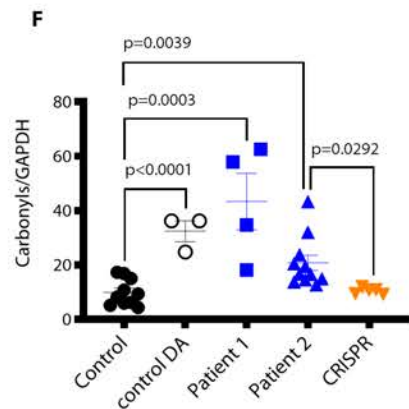
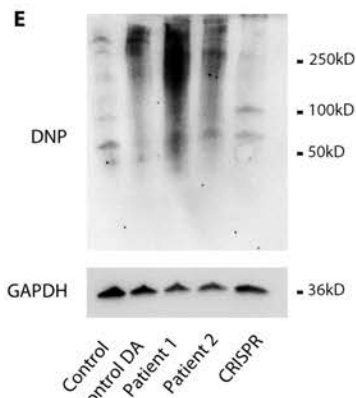
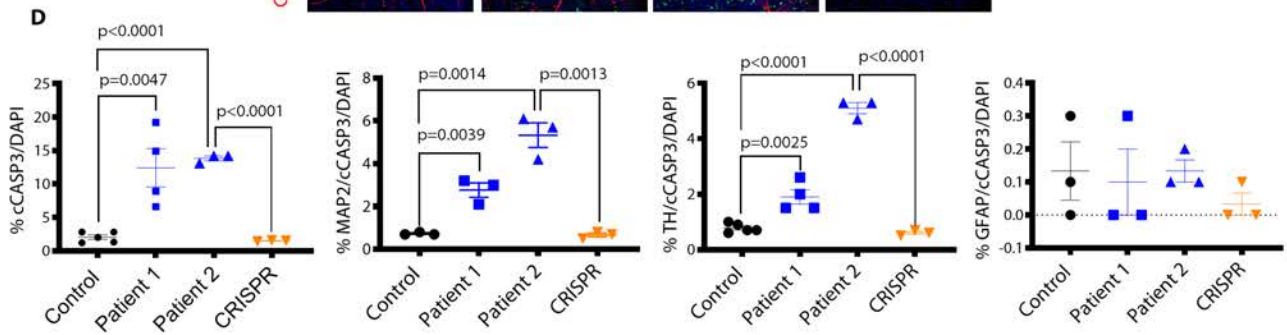
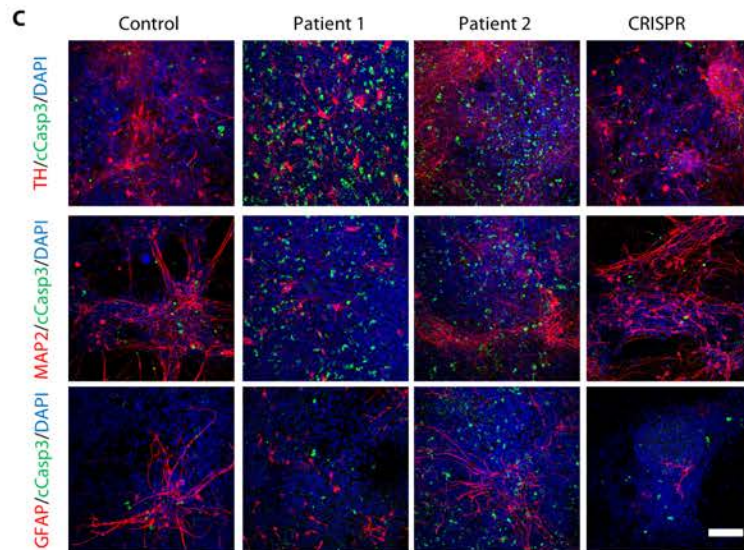
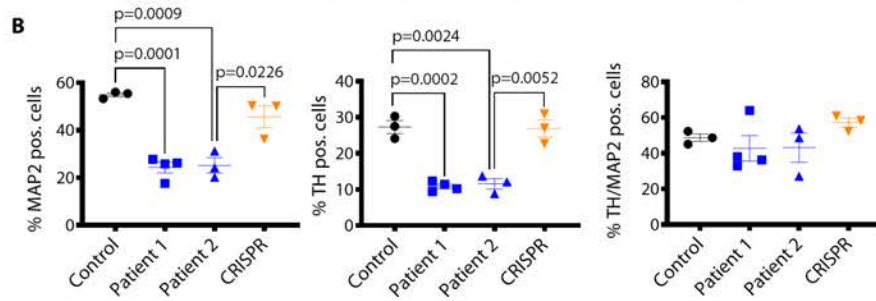
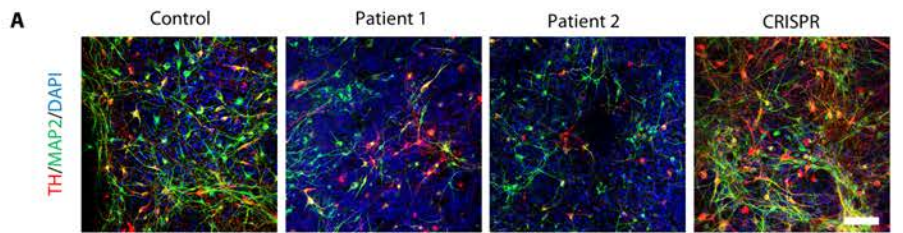
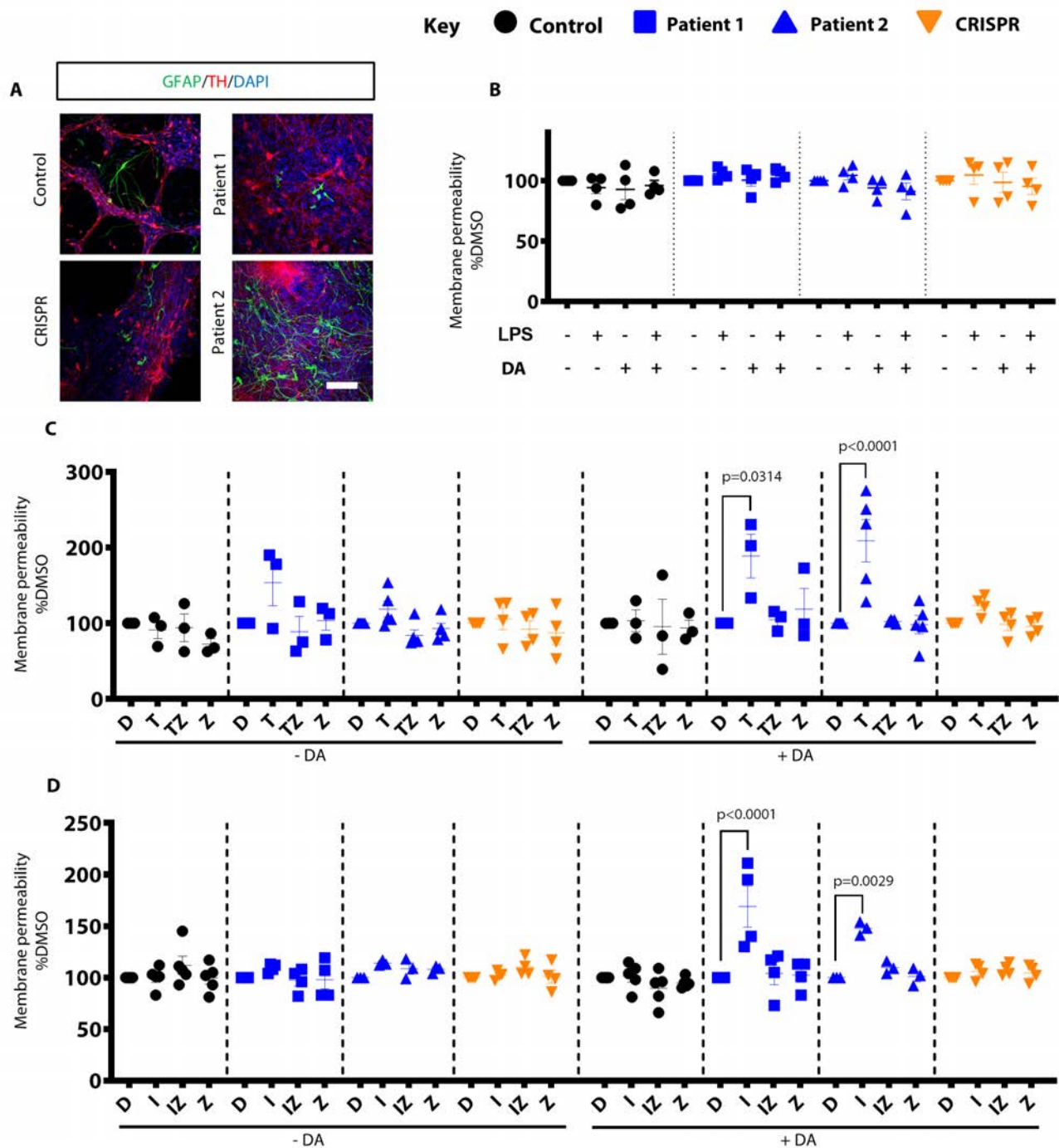


Figure 3: DAT dysfunction in DTDS is associated with neurotoxicity and apoptotic neurodegeneration

A Immunofluorescence analysis for neuronal markers TH/MAP2 at d65. Nuclei were counterstained with DAPI. Scale bar 100µm. **B** Quantification of MAP2 positive, TH positive and TH/MAP2 double positive neurons for control, Control, Patient 1, Patient 2 and CRISPR derived neuronal populations (n = 3, 4, 3, 3 respectively). **C** Immunofluorescence analysis for TH/cCASP3, MAP2/cCASP3 and GFAP/cCASP3 at d65. Nuclei were stained for DAPI. Scale bar 100 µm. **D** Quantification of total number of cCASP3 positive cells, MAP2/cCASP3, TH/cCASP3, and GFAP/cCASP3 double positive cells in Control, Patient 1, Patient 2 and CRISPR derived neuronal populations (n = 5, 4, 3, 3 respectively; n = 3, 3, 3, 3 respectively; n = 5, 4, 3, 3; n = 3, 3, 3, 3 respectively). **E** Immunoblot of total carbonyls detected in mDA neurons at d65 derived from Control, Control treated with 100 µM dopamine (DA), Patient 1, Patient 2 and CRISPR. **F** Quantification of total carbonyls relative to GAPDH (n = 10, 3, 4, 11, 5 respectively). Error bars indicate SEM. Both DTDS lines were independently compared to controls using two-tailed Student's *t*-test.



1 Results are normalized to the DMSO condition **C,D** Membrane permeability at d65 of differentiation.
2 Cells were treated for 24 hours with DMSO (D), TNF α (T) or IL1- β (I), TNF α or IL1- β + Z-VAD-FMK
3 (TZ; IZ), or just Z-VAD-FMK (Z). Dopamine (DA) was added at concentration of 100 μ M (n = 3, 3, 5,
4 4 for each line; n = 5, 4, 3, 4 respectively). Results are normalized to the DMSO treated condition.
5 Error bars indicate SEM. ANOVA was applied to allow multiple comparisons with normalized control.

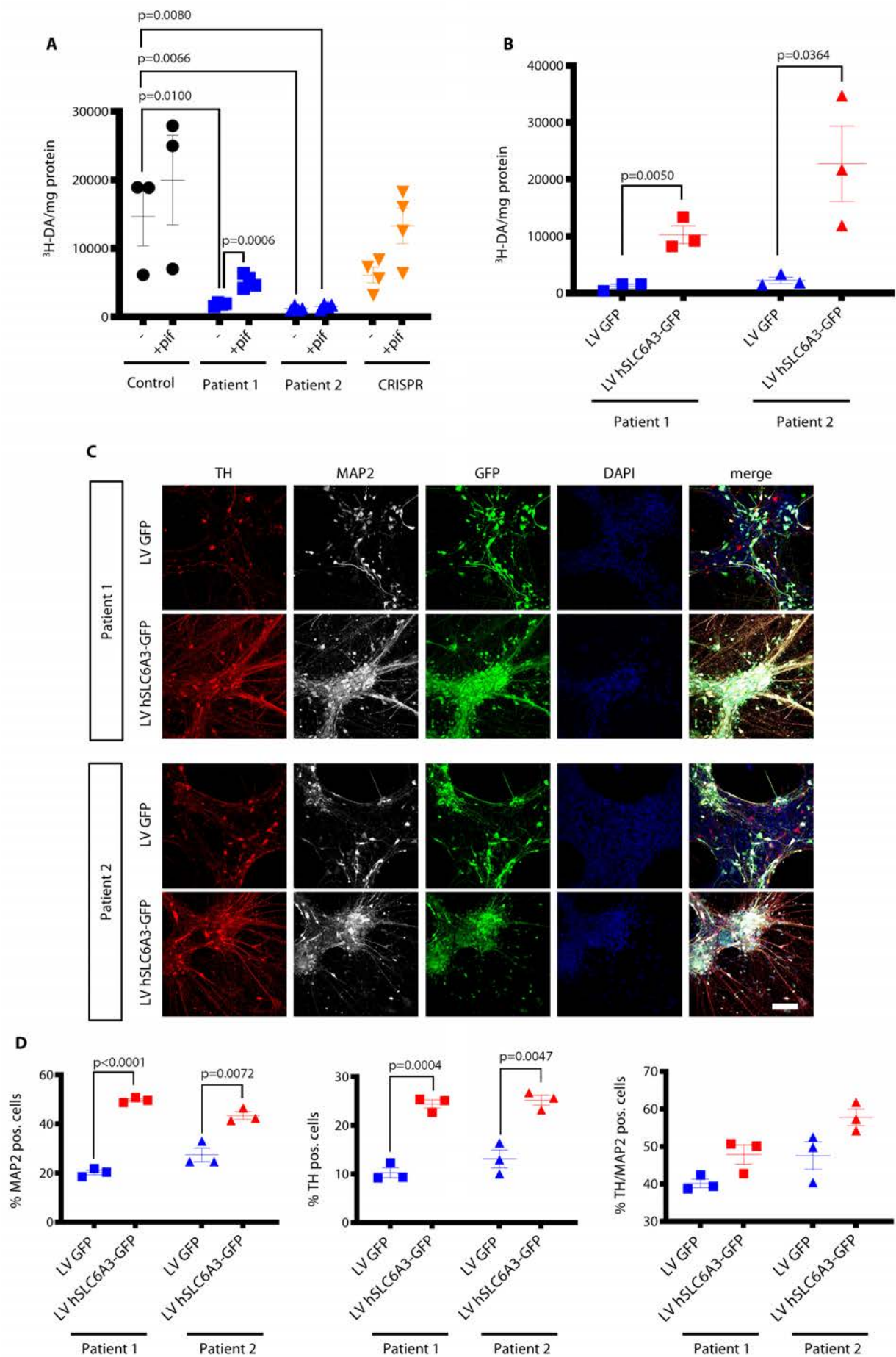


Figure 5: Loss of DAT function in DTDS can be restored both pharmacologically and using a gene therapy approach in the mDA model

A Uptake of tritiated dopamine at d65 after neurons treated for 24 hour with pifithrin- μ (pif). Values are relative to protein concentration (n = 3, 4, 4, 4 per line). **B** Measurement of tritiated dopamine uptake at d65 in patient-derived mDA neurons transduced with either a lentivirus construct expressing GFP alone (LV GFP) or human *SLC6A3* and *SLC6A3* GFP (LV hSLC6A3SLC6A3-GFP) (n = 3 for each). **C** Immunofluorescence analysis at d65 for patient-derived dopaminergic neurons transduced with LV GFP or LV hSLC6A3-GFP. Cells are stained for TH/MAP2, nuclei were counterstained with DAPI. Scale bar 100 μ m. **D** Quantification of MAP2 positive, TH positive and TH/MAP2 double positive neurons at d65 of differentiation in mDA neurons transduced with LV GFP or LV hSLC6A3SLC6A3-GFP (n = 3 for each). Both DTDS lines were independently compared to controls using two-tailed Student's *t*-test for all analyses.

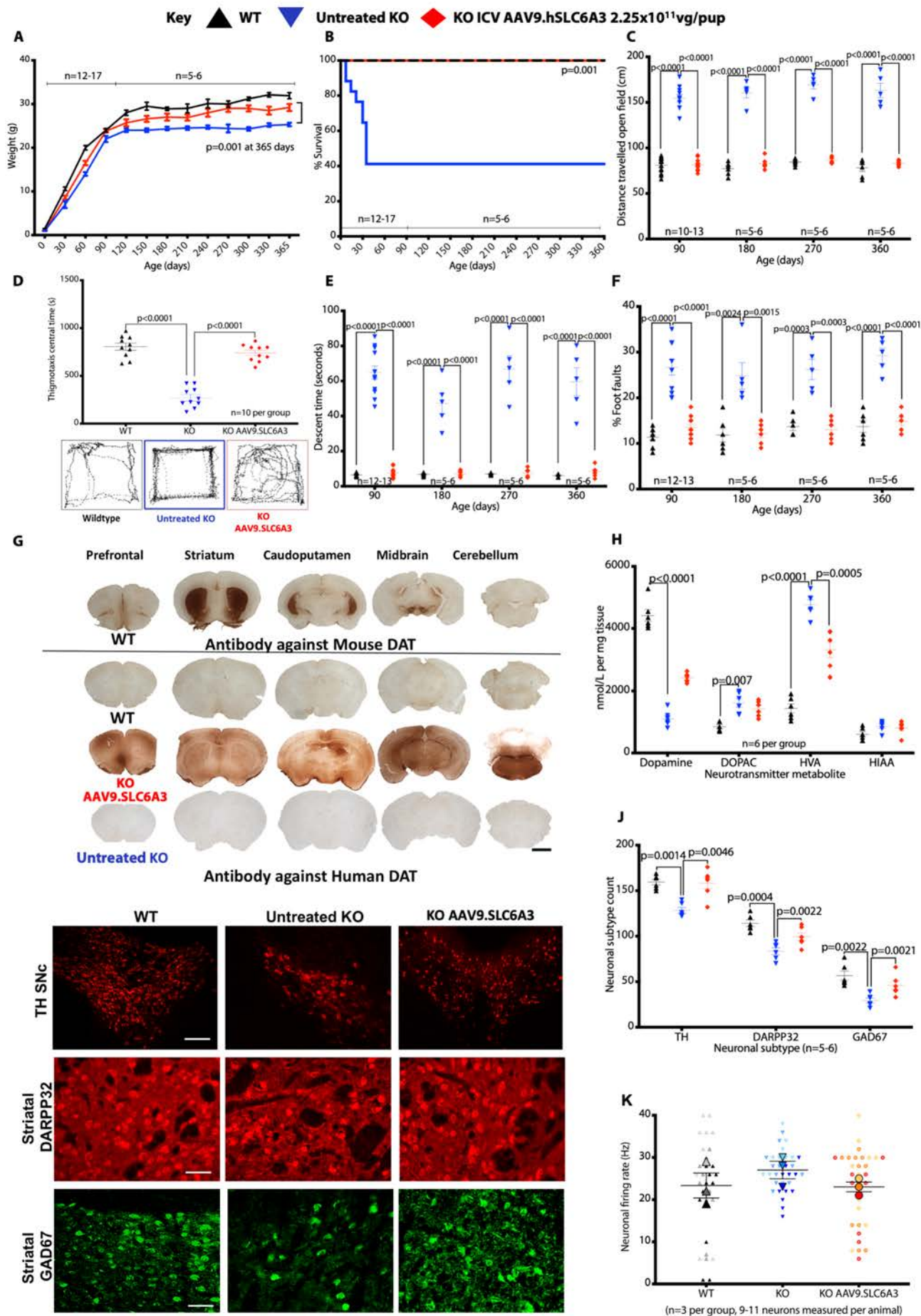


Figure 6: Neonatal intracerebroventricular gene therapy to DAT knockouts

A Weights of mice (2.25×10^{10} vg/pup, treated knockout $n = 13$, wildtype $n = 12$, untreated knockout $n = 17$ (Data means \pm S.E.M., Student's one-tailed t -test on weight at 365 days untreated knockout versus treated) **B** Kaplan-Meier survival plot of wildtype, untreated knockout, intracerebroventricular hDAT gene therapy treated knockout (Logrank, Mantel-Cox test). **C** Locomotor assessment of mice in open field with distance travelled **D** Central time and thigmotaxis with representative open field traces for each group **E** vertical pole descent time **F** foot faults (Data means \pm S.E.M., two-way ANOVA, Log transformed data for % foot fault, Bonferroni's multiple comparison, group sizes as stated). **G** Representative immunostaining for mouse DAT in wildtype mice for physiological expression reference. Immunostaining for human DAT in treated knockout, untreated knockout and wildtype mice (scale bar 1 mm, $n = 5$ per group). **H** Dopamine and serotonin neurotransmitter metabolites from whole brain homogenates analysed by HPLC. (Data means \pm S.E.M., two-way ANOVA, Bonferroni's multiple comparison, $n = 6$ per group). **I** Representative immunofluorescence for cell types TH mDA neurons (scale bar 250 μ m), striatal DARPP32 and GAD67 neurons (scale bar 100 μ m) in wildtype, untreated knockout and knockout hDAT treated mice ($n = 5-6$ per group). Data means \pm S.E.M. **J** Quantification of TH, DARPP32 and GAD67 neurons in wildtype, untreated knockout and knockout hDAT treated mice (Data means \pm S.E.M. two-way ANOVA, Tukey's multiple comparison, $n = 5$ per group). **K** Patch clamp electrophysiology of striatal medium spiny neurons ($n = 3$ animals per group with 9-11 neurons measured per animal). Data means per animal \pm S.E.M of group.

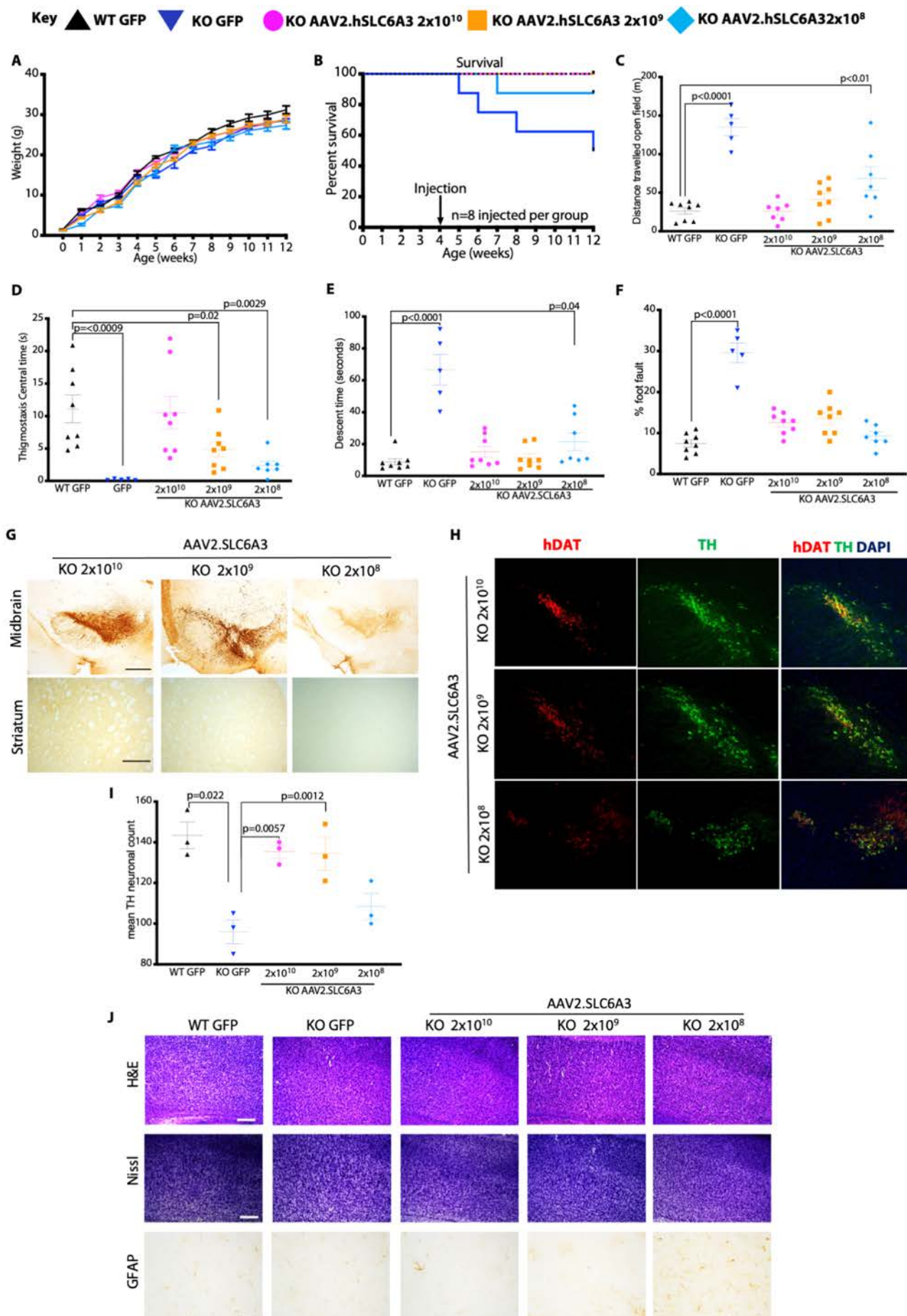


Figure 7: Adult stereotactic AAV2 gene therapy to DAT knockout mice 2 log dose-ranging study.

A Weights of mice receiving stereotactic injected AAV2.SLC6A3 vector treated knockouts at 3 dosages. 2×10^{10} , 2×10^9 , 2×10^8 vg/mouse. Control wildtype and knockout animals received AAV2.GFP vector 2×10^{10} vg/mouse (data means \pm S.E.M, n = 8 per group). **B** Kaplan-Meier survival plot of wildtype AAV2.GFP, knockout AAV2.GFP and treated knockout AAV2.SLC6A3 2×10^{10} , 2×10^9 , 2×10^8 vg/mouse dosage groups **C** Locomotor assessment of mice at 12 weeks (8 weeks post gene transfer) in open field with distance travelled **D** thigmotaxis central time **E** vertical pole descent time **F** foot faults (Data means \pm S.E.M., two-way ANOVA, Log transformed data for % foot fault, Bonferroni's multiple comparison n = 5-8 animals per group). **G** Representative immunostaining of midbrain and striatum for human DAT in AAV2.SLC6A3 treated knockout mice at 2×10^{10} , 2×10^9 , 2×10^8 vg/mouse dosages, (scale bar 100 μ m, n=3 per group). **H** Representative double labelled immunofluorescence for TH mDA neurons coexpressing hDAT in AAV2.SLC6A3 treated knockout mice at 2×10^{10} , 2×10^9 , 2×10^8 vg/mouse (scale bar 250 μ m, n = 3 per group). **I** Quantification of TH neurons of AAV2.SLC6A3 treated knockouts at 2×10^{10} , 2×10^9 , 2×10^8 vg/mouse (Data means \pm S.E.M., two-way ANOVA, n = 3 group). **J** Neurohistological panel showing frontal cortex of wildtype AAV2.GFP, knockout AAV2.GFP and knockout AAV2.SLC6A3 treated mice at 2×10^{10} , 2×10^9 , 2×10^8 vg/mouse. Representative images of Haematoxylin and Eosin and Nissl stain (scale bar 250 μ m). Immunohistochemistry for GFAP in frontal cortex (scale bar 100 μ m, n = 3 per group for each panel).

Supplementary Materials

Material and Methods

iPSC generation and maintenance

Generation of iPSCs from patient dermal fibroblasts was approved by the Local Research Ethics Committee (Reference 13/LO/0171). Written informed consent was obtained from all patients. Fibroblasts were cultured from skin biopsies and maintained in DMEM (Gibco), 10% FCS (Gibco), 2 mM L-glutamine (Gibco), 1% MEM non-essential amino acids (Gibco), and 100 u/ml penicillin 100 μ g/ml streptomycin (P/S, Gibco). Age-matched healthy control fibroblasts were obtained from the MRC Centre for Neuromuscular Disorders Biobank. Fibroblasts were reprogrammed using the commercially available CytoTune-iPS Reprogramming kit (Invitrogen), containing four CytoTune

Sendai reprogramming vectors (hOct3/4, hSox2, hKlf4, hc-Myc). Viral transduction was performed on cells at 90% confluency ($1-1.5 \times 10^5$ /well), in 12 well plates. After 6 days, infected cells were harvested with TrypLE (Invitrogen) and 8,000 cells/6 well plate were seeded onto gamma-irradiated mouse embryonic fibroblasts (MEF). One day later, medium was changed to knockout-DMEM (Gibco), 20% serum replacement (Gibco), 2 Mm L-glutamine, 50 μ M 2-mercaptoethanol (Gibco), MEM non-essential amino acids, P/S, and 10ng/ml bFGF (Gibco). From day 13, MEF-conditioned medium was added to the culture. Colonies with iPSCs-morphology developed around 30 days after transduction. Eight to ten independent colonies per patient were collected and expanded by manual passaging. Between passage 15 and 20, 3 colonies per patient were converted to mTeSR1 medium (Stemcell technologies) onto Matrigel (Corning) coated plates. Derived iPSCs were maintained in mTeSR1 on matrigel and regularly passaged with EDTA 0.02% solution. Two colonies per patient (Patient 1-03 and Patient 1-08; Patient 2-01 and Patient 2-06) and age-matched healthy control (Control-05 and Control-03) were characterized and differentiated into mDA neurons to exclude clonal variability. One clone per patient and age-matched healthy control was used for further studies unless otherwise stated.

Generation of isogenic control by CRISPR/Cas9 gene editing

For DTDS patient line Patient 2-01 harbouring homozygous *SLC6A3* variant c.1184C>T, a CRISPR/Cas9 corrected line (CRISPR) was generated by Applied StemCell, Inc (Milpitas). Briefly, two guide RNA (gRNA) candidates were cloned and tested in HEK293 cells to evaluate Cas9-mediated cleavage efficiency in vitro (Supplementary Table 1). Patient 2-01 iPSCs were transfected (Neon transfection system, Invitrogen) with gRNAs and single-stranded oligo donor (ssODN). Single cells were seeded in 96-well plates and cultured for 14 days before expanding and culturing in 24 well plates. Each clone was isolated and genomic DNA extracted for PCR amplification of the mutated sequence (Supplementary Table 1). PCR products were subsequently sequenced to confirm bi-allelic correction of the homozygous *SLC6A3* mutation.

Direct Sanger sequencing

DNA from all iPSCs lines was extracted using a commercially available kit (DNeasy Blood & Tissue kit, Qiagen), following manufacturer instructions. Direct Sanger Sequencing of genomic DNA extracted from control, patient-derived, and CRISPR-corrected isogenic iPSCs was undertaken to confirm genotype. Primer pairs for exon-specific PCR amplification were designed using Primer3 software (<http://bioinfo.ut.ee/primer3/>), and the *SLC6A3* DNA template (Ensembl genome browser: <http://www.ensembl.org/index.html>, NCBI Genome Reference Consortium (GRC)h38.p10;chromosome 5: 1,392,790-1,445,430; NM_001044.4). Primer sequences and PCR

conditions are available on request. PCR products were purified with MicroCLEAN (WebScientific). The purified PCR product was subsequently sequenced in both forward and reverse directions using the BigDye Terminator Cycle Sequencing System (Applied Biosystems). Sequencing reactions were carried out on an ABI PRISM 3730 DNA Analyzer (Applied Biosystems). The results were analyzed using Sequencher (<https://www.genecodes.com>) and Chromas software (<http://technelysium.com.au/wp/chromas>)

Assessment of genome integrity

Genome integrity was assessed by Illumina Human OmniExpress24 array using genomic DNA, as per manufacturer's instructions, and Karyostudio software was used to generate karyograms (Illumina).

Analysis of pluripotency by in vitro spontaneous differentiation

Embryoid bodies (EBs) were generated by harvesting cells with TrypLE and plated onto non-adherent bacterial dishes to a concentration of 1.5×10^5 per cm^2 in knockout-DMEM medium, 20% serum replacement, 2 mM L-glutamine, 1% MEM non-essential amino acids, 50 μM 2-mercaptoethanol (Gibco), 1 μM ROCK-inhibitor (thiazovivin for the first 2 days, Cambridge Bioscience). In order to direct neuroectodermal and endodermal fate, EBs were plated at day 4 on matrigel-coated dishes and maintained in the same media (described above for EB generation) until day 16. For mesodermal differentiation, EBs were plated onto 0,1% galantine (Sigma-Aldrich) coated dishes in DMEM, 20% FCS, and 2 mM L-glutamine for 16 days, until cells were analyzed by immunofluorescence (see below).

Analysis of pluripotency by teratoma assay

iPSCs were harvested using TrypLE (Invitrogen) and re-suspended as single cell suspension in 100 μl of mTeSR1 medium with added matrigel and ROCK-inhibitor (Thiazovivin). Two million cells were then injected subcutaneously into the flank of Severe Combined Immunodeficient mice to assess teratoma formation. Visible tumors were collected after 4 months and processed for histological analysis. Briefly, tumors were fixed in 4% paraformaldehyde (PFA) overnight and then embedded in paraffin. 10 μm sections were cut with a microtome and processed for haematoxylin and eosin histological staining. These experiments were performed under UK Home Office license 70/8030 and approved by the UCL ethics review committee.

Analysis of pluripotency by Epi-Pluri-Score

All derived iPSCs lines were additionally analyzed with Epi-Pluri-Score (Cygenia), which compares pluripotent with non-pluripotent cells. The Epi-Pluri-Score is based on the combination of DNA methylation degree at the two CpG sites of *ANKRD46* and *C14orf115* (43).

Differentiation of iPSC in mDA neurons

iPSCs were differentiated into dopaminergic neurons using a modified version of the dual SMAD inhibition protocol (14, 15). Briefly, iPSCs were harvested using TrypLE (Invitrogen), and plated onto non-adherent bacterial dishes to a concentration of 1.5×10^5 per cm^2 to generate EBs in DMEM/F12:Neurobasal (1:1), N2 (1:100), B27 minus vitamin A (1:50) (Invitrogen), 2 mM L-glutamine and ROCK-inhibitor (Thiazovivin) for the first two days. EBs were plated on day 4 onto polyornithine (PO; 15 $\mu\text{g}/\text{ml}$; Sigma), fibronectin (FN; 5 $\mu\text{g}/\text{ml}$ Gibco) and laminin (LN; 5 $\mu\text{g}/\text{ml}$; Sigma) coated dishes in DMEM/F12:Neurobasal (1:1), N2 (1:200), B27 minus vitamin A (1:100), 2 mM L-glutamine. From day 0 to day 6, media was supplemented with: 10 μM SB431542 (Tocris Bioscience), 100 nM LDN193189 (Stemgent Inc.), 0.8 μM CHIR99021 (Tocris Bioscience) and 100 ng/ml hSHH-C24-II (R&D Systems). On day 2, 0.5 μM purmorphamine (Cambridge Bioscience) was added. SB431542 was withdrawn on day 6 and all other supplements were continued until day 9 of differentiation. On day 11, cells were either processed for midbrain precursor analysis or harvested with Accumax and re-plated on PO/FN/LN coated dishes in droplets of $1-1.5 \times 10^4$ cells per μl in Neurobasal B27 minus vitamin A (1:50), 2 mM L-glutamine, 0.2 mM ascorbic acid (AA) and 20 ng/ml BDNF (Miltenyi Biotech). On day 14 of differentiation, 0.5 mM dibutyryl c-AMP (Sigma-Aldrich) and 20 ng/ml GDNF (Miltenyi Biotech) were added. On day 30 of differentiation, cells were re-plated (following the same protocol as described for day 11) in the same medium, and the γ -secretase inhibitor DAPT (10 μM , Tocris) was added until day 65 of differentiation, when cells were harvested for further analysis.

Immunocytochemistry

Cells were fixed in 4% paraformaldehyde. Immunofluorescence (IF) for assessment of pluripotency, spontaneous in vitro differentiation experiments and day 11 mDA precursors was performed in 0.1% triton X-100, 10% fetal calf serum (FCS), 1x phosphate-buffered saline (PBS) except for the surface antibodies TRA-1-60 and TRA-1-81 where triton X-100 was omitted. Immunostaining of samples at day 65 of differentiation was performed in buffer solution with 0.3% triton X-100, 10% FCS, 1x PBS, except for the anti-DAT antibody where 10 % normal goat serum was used instead of FCS. After blocking for 30 min at room temperature, all primary antibodies (Supplementary Table 2) were incubated overnight at 4°C. Cells were then washed three times with 1x PBS and incubated with the

1 respectively species-specific secondary antibodies labelled with Alexa 488, Alexa 594 or Alexa 647
2 (all from Invitrogen), for 45 min at room temperature. Nuclei were stained with DAPI for 5 min at room
3 temperature. Cells, which had undergone differentiation for 65 days, were seeded on Lab-Tek slides
4 (Nunc). After immunofluorescence, coverslips were mounted with ProLong Gold Antifade Mountant
5 (Invitrogen).

6 Imaging was performed with the Olympus IX71 inverted TC scope for assessment of pluripotency
7 markers in iPSC, spontaneous in vitro differentiation of iPSC and day 11 mDA precursors. A
8 multiphoton confocal microscope (Zeiss LSM880) was used for all other IF studies. A Zeiss Axioplan
9 microscope was used for bright-field microscopy.

10 For quantification, 4 random fields were imaged from each independent experiment, and either 1200
11 or 1800 randomly selected nuclei, depending on the analysis, were quantified using ImageJ software
12 (National Institutes of Health).

13 **Quantitative Real Time PCR (qRT-PCR) Analysis**

14 RNA was purified from cells using the RNeasy mini kit (Qiagen) following the manufacturer's
15 instructions. Contaminating DNA was removed from total RNA (1 µg) using the DNaseI purification
16 kit (Invitrogen), before performing reverse transcription using Superscript III (Invitrogen) to generate
17 cDNA. Sendai virus clearance PCR was performed using manufacturer-recommended oligomers
18 (Invitrogen).

19 qRT-PCR analysis was performed using the StepOnePlus Real-Time PCR System (Applied
20 Biosystems). The qRT-PCR reaction was prepared using 1x MESA Blue qPCR MasterMix Plus for
21 SYBR Assay (Eurogentec), 0.1 µl ROX Reference Dye (Invitrogen), 9 µL cDNA (dilution 1:25) and
22 500 nM of each primer (Supplementary Table 3). All reactions were performed in technical triplicates
23 using the following conditions: denaturation of 95°C for 5 minutes, followed by 40 cycles of 15 seconds
24 denaturation at 95°C and 1 minute annealing/extension at 60°C. Relative quantification of gene
25 expression was determined using the $2^{-\Delta\Delta C_t}$ method with glyceraldehyde-3-phosphate dehydrogenase
26 (*GAPDH*) as a housekeeping reference gene, and normalized to age-matched control lines. In order
27 to assess ubiquitous expression of the mDA marker PITX3, 10 samples at day 65 of differentiation for
28 lines C-05, P1-03, P2-01 and CR-18 were processed. The distribution of mRNA content was then
29 examined for normality with D'Agostino Pearson, Shapiro-Wilk and Kolmogorow Smirnov statistical
30 tests.

1 **In vitro electrophysiology**

2 Current-clamp recordings were undertaken on mDA at day 65 after differentiation, the internal solution
3 contained (in mM): 126 K-gluconate, 4 NaCl, 1 MgSO₄, 0.02 CaCl₂, 0.1 BAPTA, 15 glucose, 5 HEPES,
4 3 ATP-Na₂, 0.1 GTP-Na, pH 7.3. The extracellular (bath) solution contained (in mM): 2 CaCl₂, 140
5 NaCl, 1 MgCl₂, 10 HEPES, 4 KCl, 10 glucose, pH 7.3. D-(-)-2-amino-5-phosphonopentanoic acid (D-
6 AP5; 50 μ M), 6-cyano-7-nitroquinoxaline-2,3-dione (CNQX; 10 μ M) and picrotoxin (PTX; 30 μ M) were
7 added to block synaptic transmission. Experiments were performed at room temperature (22-24°C).
8 Neurons with unstable resting potential (or >-50mV), bridge-balance >20 M Ω and/or holding current
9 >200 pA were discarded. Bridge balance compensation was applied and the resting membrane
10 potential was held at -70 mV. Spontaneous action potentials (APs) were triggered holding the neurons
11 around -60mV/-55mV. Current steps protocol was used to evoke APs injecting 500ms long
12 depolarizing current steps of increasing amplitude (Δ 10pA). Neurons with repetitive oscillatory
13 spontaneous APs and repetitive evoked APs were considered to be functional mature dopaminergic
14 neuron (10-20% of patched neurons). Recordings were acquired using a Multiclamp 700A amplifier
15 (Axon Instruments, Molecular Devices) and a Power3 1401 (CED) interface combined with Signal
16 software (CED), filtered at 10 kHz and digitized at 50 kHz.

17 **Tritiated dopamine uptake assay**

18 [³H]Dopamine (³H-DA) uptake measurements were performed on derived mDA neurons at day 65 of
19 differentiation in 12 well dishes as described previously (44). Briefly, cells were washed three times in
20 Dulbecco's phosphate-buffered saline with calcium and magnesium (D-PBS+Ca+Mg) (Invitrogen).
21 ³H-DA (Perkin Elmer) was diluted in D-PBS+Ca+Mg to 10 nM with or without 10 μ M mazindol (Sigma).
22 Cells were incubated for ³H-DA solution for 15 minutes. The reactions were stopped by adding ice-
23 cold D-PBS+Ca+Mg. Cells were washed twice more and sodium hydroxide (NaOH) added to lyse
24 cells for 1 hour at room temperature. Cells were scraped and transferred into scintillation vials and 1
25 ml of scintillation fluid (Perkin Elmer) added. Radioactivity was quantified using a scintillation counter
26 (Beckman Coulter). Results were normalized to protein content measured in a sample of the cell
27 lysate using the bicinchoninic acid (BCA) method.

28 **High Performance Liquid Chromatography (HPLC)**

29 Phenol red free media was collected from day 65 mDA neurons and mixed with perchloric acid to a
30 final concentration of 0.4 M. Samples were incubated for 10 min at 4°C in the dark, centrifuged at
31 12000 \times g for 5 min at 4°C, and supernatant was collected for analysis by HPLC.

1 Mouse brains were harvested immediately following transcardial perfusion with PBS. The right
2 hemisphere was harvested and snap frozen on dry ice for brain homogenisation. The brains were
3 collected and weighed. The hemisphere was transferred to cold glass tissue homogenizer on wet ice
4 and 8x volume of Homogenisation buffer (2mL 0.8M perchloric acid, 40 μ L EDTA 0.1 mM and 6 mL
5 H₂O) was added. The tissue was homogenised in glass homogeniser in wet ice. The brain
6 homogenates were transferred into a 1.5mL Eppendorf using a Pasteur pipette. The homogenate was
7 incubated at 4°C then centrifuged at 13000rpm for 5 minutes before analysis. Dopamine, DOPAC,
8 HVA, and HIAA were quantified using reverse-phase HPLC (45). Briefly, the column consisting on
9 silica with 18 carbon chains was maintained at 27°C and the flow rate was kept at 1.5 ml/min. The
10 mobile phase was aqueous with 16% methanol, 20 mM sodium acetate trihydrate (pH 3.45), 12.5 mM
11 citric acid monohydrate, 0.1 mM EDTA sodium and 3.35 mM 1-octanesulfonic acid. The detection
12 electrode (Coulchem 2015) was maintained at 450 mV and the screening electrode at 20 mV were
13 injected the system. Peak areas, from the electrochemical detector, were quantified with EZChrom
14 Elite chromatography data system software, version 3.1.7 (JASCO UK).

15 Immunoblotting

16 Proteins were extracted from cells and mouse brain tissue in ice-cold RIPA lysis and extraction buffer
17 (Sigma-Aldrich) supplemented with protease inhibitor (Roche). Protein concentration was measured
18 with Pierce BCA Protein Assay kit (Thermo Scientific): 10 μ g of protein was denatured with Laemmli
19 buffer (Bio-Rad Laboratories) with dithiothreitol (DTT). Proteins were separated with Mini-PROTEAN
20 TGX Stain Free Gels (Bio-Rad Laboratories) and transferred to a Trans-Blot Turbo Transfer
21 membrane (Bio-Rad Laboratories). After blocking in 5% milk, 1x PBS, 0.1% Tween for 1 hour at room
22 temperature, membranes were incubated with primary antibodies (Supplementary Table 2) at 4°C
23 overnight. Membranes were then incubated with the secondary anti-rabbit horseradish peroxidase-
24 conjugated antibody at a dilution of 1:3000 (Cell Signalling). Immunoreactive proteins were visualized
25 with Chemidoc MP (Bio-Rad Laboratories). In order to evaluate the total amount of endogenous
26 protein and control for equal loading, membranes were reprobed for GAPDH, after clearance with
27 Restore Western Blot Stripping Buffer (Thermo Scientific). CSF sample protein concentrations were
28 measured with Pierce BCA Protein Assay kit (Thermo Scientific) and 10 μ g denatured with Laemmli
29 buffer with dithiothreitol (DTT). Human Transferrin was probed in CSF for equal loading. The intensity
30 of immunoreactive bands was analyzed using ImageJ software (National Institutes of Health). The
31 density of the bands was normalized to GAPDH. Results are reported as means \pm SEM of
32 independent experiments, the number of which is stated for each experiment in the respective figure
33 legend.

1 **Protein carbonyl measurement**

2 Protein carbonyls were measured at day 65 of differentiation. Control mDA neurons were treated with
3 100 µM dopamine (Sigma-Aldrich) for 48 hours in order to expose cells to the effects of dopamine
4 metabolites. Proteins were extracted as described above. To prevent oxidation of protein during
5 extraction, 1% 2-mercaptoethanol (Gibco) was added to the lyses buffer. Protein carbonyls were
6 detected with the OxyBlot Protein Oxidation Detection kit (Millipore) according to the manufacturer's
7 instructions. Samples were then separated and immunoblotted as described above.

8 **Cytometric bead array**

9 Five anonymized control paediatric CSF samples (with normal CSF neurotransmitter profiles) were
10 obtained from the Neurometabolic Laboratory (National Hospital for Neurology and Neurosurgery,
11 Queen Square, London). Five anonymized, genetically-confirmed CSF samples from patient with
12 DTDS were also obtained. All samples were processed and stored in accordance with the UK Royal
13 College of Pathologists guidelines. Using standardized protocols, CSF neurotransmitter analysis was
14 undertaken using HPLC with electrochemical detection and reversed phase column (20). CSF
15 cytokine concentration was measured with the cytometric bead array Human Th1/Th2/Th17 Kit (BD
16 Bioscience) following manufacturer's indications. Analysis was performed using the flow cytometer
17 BD LSRII. CSF TNF concentration was determined after interpolation with a calibration curve.

18 **Cytotoxicity assay**

19 On day 65 of differentiation, iPSC-derived neurons were incubated for 24 hours with or without 100
20 µM dopamine (Sigma-Aldrich). They were then treated with: dimethyl sulfoxide (DMSO, Sigma-
21 Aldrich), 1 µg/ml lipopolysaccharide (LPS, Sigma-Aldrich), 100 ng/ml tumor necrosis factor alpha
22 (TNFα, PeproTech), 100 ng/ml interleukin beta (IL-1β PeproTech) and 30 µM pan-caspase inhibitor
23 Z-VAD-FMK (R&D Systems) for 24 hours. Protease release was measured using the CytoTox-Glo
24 Cytotoxicity Assay (Promega) according to the manufacturer's instructions.

25 **Treatment of neuronal cultures with Pifithrin-µ**

26 Derived mDA neurons at day 65 of differentiation were treated with 1 µM pifithrin-µ (Sigma-Aldrich)
27 for 24 hours. Medium was subsequently removed and the uptake of ³H-DA was assessed as
28 described above.

Lentiviral vector generation

The human *SLC6A3* coding sequence (NM_001044.4) and human Synapsin 1 promoter cDNA (46) were cloned into a pCCL lentiviral expression vector (47) using standard cloning methods. To facilitate identification of transduced cells, an internal ribosomal entry site (IRES2) and enhanced green fluorescent protein (EGFP) coding sequence were then inserted downstream of the h*SLC6A3* sequence. Control plasmid was generated using the CCL-hSyn.IRES2.GFP.WPRE as a template with the primers 3F and 3R in Supplementary table 4. All primers used for cloning are listed in Supplementary Table 4. VSV-G pseudotyped lentiviral vectors (LV) were produced using a 2nd generation packaging system (48). For virus titration, 1×10^5 HeLa cells were plated into each well of a 6 well plate and transduced with a range of volumes of the concentrated lentivirus. Seventy-two hours after transduction, HeLa cell genomic DNA was extracted and the proviral titre was calculated by qPCR, as described previously (48) using primers listed in Supplementary Table 4. Titres ranged 7×10^8 - 2×10^9 vg/mL. As described, mDA neural cells were differentiated for 23 - 29 days, before transduction with LV at the designated multiplicity of infection (MOI). LV containing media was replaced with fresh culture medium 24 hours after transduction.

AAV vector generation

hSyn.GFP plasmid containing single-stranded AAV2 inverted terminal repeats was used to generate the control AAV vectors. The human h*SLC6A3* cDNA was cloned into this AAV expression vector using standard cloning techniques (Primers supplementary table 4). Recombinant single stranded AAV2/9 (referred to as AAV9, throughout) and AAV2 serotype vectors encoding h*SLC6A3* or *GFP* were generated by the standard triple plasmid transfection method as described previously (49). Cell lysates of transfected 293T cells and vector purified through affinity chromatography on an ÄKTAprime plus (GE Healthcare) with Primeview 5.0 software with a POROS CaptureSelect AAVX resin (Thermo Fisher Scientific) All vector preparations were titred by RT-qPCR using the Applied Biosystems StepOne Plus Real-Time PCR system. Five µl of AAV vector was digested in 45µl DNase I buffer and 10units DNase I (NEB) and incubated at 37° C for 1 hour followed by Proteinase K treatment (Invitrogen). PCR reactions were performed in 20 µl of final volume using the Luna Taqman qPCR mix (NEB). Primers and probe used targeted transgenes GFP or h*SLC6A3* are listed in Supplementary table 4 serial dilutions of linearized plasmid were used to generate a standard curve. All vectors were produced to titres 1×10^{13} - 1×10^{14} vg/mL.

1 **Animal welfare**

2 All animal experiments were performed in compliance with UK Home Office and the Animal (Scientific
3 Procedures) Act of 1986, and within the guidelines of University College London ethical review
4 committee. Outbred CD1 dams (Charles River) were time-mated to generate P0-P1 litters for marker
5 gene studies. Pups were weaned at P21 and euthanised for tissue analysis at P35.

6 The DAT knockout mouse model used in this study has been described previously (24,25).
7 Heterozygous mice were time mated to generate mixed genotype litters. Pups were genotyped at P0
8 using primers (JAH1F 5' CCCGTCTACCCATGAGTAAAA, JAH2 5' CTCCACCTTCCTAGCACTAAC,
9 NEO1 5' TGACCGCTTCCTCGTGC). Intracerebroventricular gene therapy was delivered to knockout
10 pups by P1.

11 **Neonatal Intracerebroventricular injection**

12 The intracerebroventricular injections were directed to the lateral ventricle of P0-1 mice as described
13 previously (50). A 33-gauge needle (Hamilton) was inserted perpendicularly at the injection site to a
14 depth of 3 mm and 5 µl of vector was administered over 5 seconds into the lateral ventricle. The pup
15 was returned to dam promptly.

16 **Adult Stereotactic injection**

17 Animals underwent stereotactic surgery at 28-30 days post-natal days. Mice were anaesthetized in
18 induction chamber with Isoflurane/ O₂ mixture at a ratio of 3:2. The head was shaved and mice were
19 placed in a stereotactic frame (Panlab, Harvard Apparatus) on homeothermic heating mat system
20 (Panlab, Harvard Apparatus). Anaesthesia was maintained by continuous nose cone isoflurane/O₂
21 mixture at 2.5:2.5. Mid-line scalp incision was made and burr holes drill with hand microdrill (Panlab,
22 Harvard Apparatus). Injections bilaterally targeted the SN antero-posterior (AP) – 3.2 mm, medio-
23 lateral (ML) ± 1.2 mm relative to the Bregma and dorso-ventral (DV) 4.3 mm relative to the dural
24 surface (Paxinos and Franklin) (51). AAV2 vectors were delivered through 33 gauge Hamilton needle
25 and 5 µl syringe infused at 100nL per minute and needle withdrawn gradually over 30 minutes.
26 Dosages were injected in 2 µl volume bilaterally (dosage ranging from 2 x 10⁸ to 2 x 10¹⁰ vg/mouse).
27 Wound was closed with 4.0 vicryl suture (Ethicon). All animals were single housed and monitored
28 daily for 1 week for general health status. All animals fully recovered from surgery and were all
29 included in the study.

1 **Behavioral studies**

2 Mice were weighed regularly and assessed for changes in motor phenotype. Spontaneous open field
3 locomotor activity and thigmotaxis were recorded (300mm width x 300mm length x 200mm height) in
4 an illuminated quiet room for 15 minutes. The distance travelled for 15 minutes was recorded and
5 quantified using motion tracking software (Smart 3.0, Panlab, Harvard Apparatus).

6 Vertical pole test places mouse upwards facing on the top of a vertical wooden rough surfaced pole
7 (diameter 1 cm, height 50 cm). Each mouse was habituated to the pole on the day prior to testing,
8 then allowed to descend five times on a single session. The total time until the mouse reached the
9 floor with its four paws was recorded. If the mouse was unable to descend or fell or slipped down, the
10 default value of 120 seconds was taken into account. The foot fault test was performed to evaluate
11 the motor accuracy abilities of the mice to place the forepaws on a wire while moving along a metal
12 grid. The mice are placed on raised a metal grid with 10mm x10mm square grids (200mm width x
13 300mm length) and allowed to spontaneously explore the grid for 5 minutes. The animals were filmed
14 and the frequencies of slips for the forelimbs and hindlimbs was recorded with total number of steps
15 during locomotion were recorded. A positive foot fault was considered when the paw slip caused the
16 animal to fall between rungs. Movie assessors were blinded to genotype and treatment group.

17 **Histological and immunohistochemical analyses of mouse tissues**

18 Mice were culled by terminal transcardial perfusion using PBS. Collected tissues (brain and visceral
19 organs) were halved to allow for different processing techniques. Brains used for
20 immunohistochemistry were post-fixed in 4% PFA for 48 hours and transferred into 30% sucrose
21 solution for cryoprotection at 4°C until sectioning. Brains were mounted on a freezing microtome
22 (ThermoFisher HM430) at 40 µm thickness in either coronal or sagittal planes. Free-floating
23 immunohistochemistry-based analyses was performed as previously described (52) with brain
24 sections selected at 240 µm intervals for whole-brain immunohistochemistry. Briefly, free-floating
25 sections were blocked in 15% normal goat serum (Vector Laboratories)- tris buffered saline with 0.1%
26 triton-X (TBS-T) (Sigma) for 1 hour at room temperature and incubated in primary antibodies
27 (Supplementary Table 2) in 10% normal goat serum-TBS-T overnight at 4°C. The following day
28 sections are incubated with the respectively species-specific secondary antibodies (Vector
29 Laboratories) for 1 hour at room temperature, washed in TBS followed by incubation with Vectastain
30 avidin-biotin solution (Vector Laboratories). The reaction visualized with 3,3'-Diaminobenzidine (DAB)
31 (Sigma). DAB reaction was stopped using ice cold 1x TBS and sections washed before mounting on
32 double coated gelatinized glass slides. The mounted sections were air dried and dehydrated in 100%

1 ethanol for 10 minutes and HistoClear (National Diagnostics) for 30 minutes prior to being covered
2 with DPX mountant (VWR International) for coverslipping.

3 Conventional methods were used for Harris hematoxylin and eosin staining (Sigma-Aldrich). Brain
4 sections were mounted on chrome-gelatine-coated slides and air-dried overnight. The sections were
5 stained with filtered 0.1% Mayer's haematoxylin (Sigma-Aldrich) for 10 minutes. The slides were
6 rinsed in distilled water for 5 minutes and consequently dipped in 0.5% eosin solution. The sections
7 were washed in distilled water and subsequently dehydrated in rising concentrations of ethanol (50%,
8 70%, 95%, 100%). The slides were coverslipped with DPX mountant (VWR International).

9 For Nissl staining representative brain sections were mounted onto double coated gelatinized slides
10 and dried overnight. The sections were dehydrated in 70% ethanol overnight on the second day.
11 Slides were immersed in the 1% Cresyl violet solution (Millipore) for 3 minutes . Excess solution was
12 removed by washing twice in running water. The slides were dehydrated by consecutive immersion
13 (2 minutes each) in increasing concentrations of ethanol (70%, 90%, 96%, 96% with glacial acetic
14 acid (Sigma) 100% EtOH, isopropanol, and three washes in xylene. Slides were then coverslipped as
15 described previously.

16 For immunofluorescence brain sections were blocked in 15% goat serum for 30 minutes and then
17 incubated with primary antibodies (Supplementary Table 2) diluted in 10% normal goat serum TBS-T
18 0.3% overnight at 4°C. The sections were washed in 1xTBS and incubated for 2 hours with the
19 respectively species-specific secondary antibodies labelled with Alexa 488 and Alexa 594 (all from
20 Invitrogen) diluted in 10% normal goat serum at room temperature. Nuclei were stained with DAPI
21 (Sigma Aldrich) for 2 minutes. The brain sections were mounted onto double coated slides and
22 coverslipped using Fluoromount G (Thermofisher Scientific).

23 Light microscopy and fluorescence imaging were carried out using a Leica DM 4000 linked to Leica
24 DFC420 camera system. Confocal images were captured using a Leica TCS SP5 AOBS confocal
25 microscope. Images were analyzed with Image J software (National Institutes of Health).

26 Quantification of neurons was conducted with assessor blinded to genotype and treatment group. For
27 each animal, eighteen non-overlapping ×40 magnification images were taken through four
28 consecutive sections for each region of interest striatum and midbrain. During image capture, the
29 same camera and microscope settings were maintained. The average values of cell counting are
30 represented.

Acute slice electrophysiology

Untreated knockout, wildtype and treated knockouts were rapidly perfused with ice cold oxygenated slicing solution (in mM): 75 sucrose, 87 NaCl, 2.5 KCl, 25 NaHCO₃, 25 glucose, 7 MgCl₂, 0.5 CaCl₂. Brains were quickly dissected into ice-cold oxygenated slicing solution and were cut into 300 µm coronal slices using a VT1200S Vibrotome (Leica Biosystems). Slices were stored submerged in oxygenated recording standard aCSF (in mM): 125 NaCl, 2.5 KCl, 25 NaHCO₃, 1.25 NaH₂PO₄·H₂O, 1 MgCl₂, 2 CaCl₂, 25 glucose at room temperature for at least one hour prior to recording. All the current clamp recordings were performed in a standard external solution containing (see slice preparation section above) in presence of D-(-)-2-amino-5-phosphonopentanoic acid (D-AP5; 50 µM), 6-cyano-7-nitroquinoxaline-2,3-dione (CNQX; 10 µM) and bicuculline methiodide (30 µM) for blocking of NMDA, non-NMDA, and GABAA receptors, respectively. The internal solution contained (in mM): 126 K gluconate, 4 NaCl, 1MgSO₄, 0.02 CaCl₂, 0.1 BAPTA, 15 glucose, 5 HEPES, 3 ATP, 0.1 GTP (pH 7.2 with knockout). Resting membrane potential was hold at -70 mV for all the recordings. Neurons with leak current >100pA and Ra >20MΩ were not considered for the analysis. All recordings and analysis were carried blinded to mouse genotypes. Recordings were acquired using a Multiclamp 700A amplifier (Axon Instruments, Molecular Devices) and Signal software in conjunction with CED Power 1401-3 (CED, Cambridge Electronic Design), filtered at 10 kHz and digitized at 50 kHz. The sampling frequency was set to 20 KHz. A 500 ms step currents were injected from -20 pA to 300 pA with 10 pA increases. AP were calculated only if they crossed 0mV and they had a rising slope (dV/dt) > 20 mV/ms.

Primary neuron AAV transduction

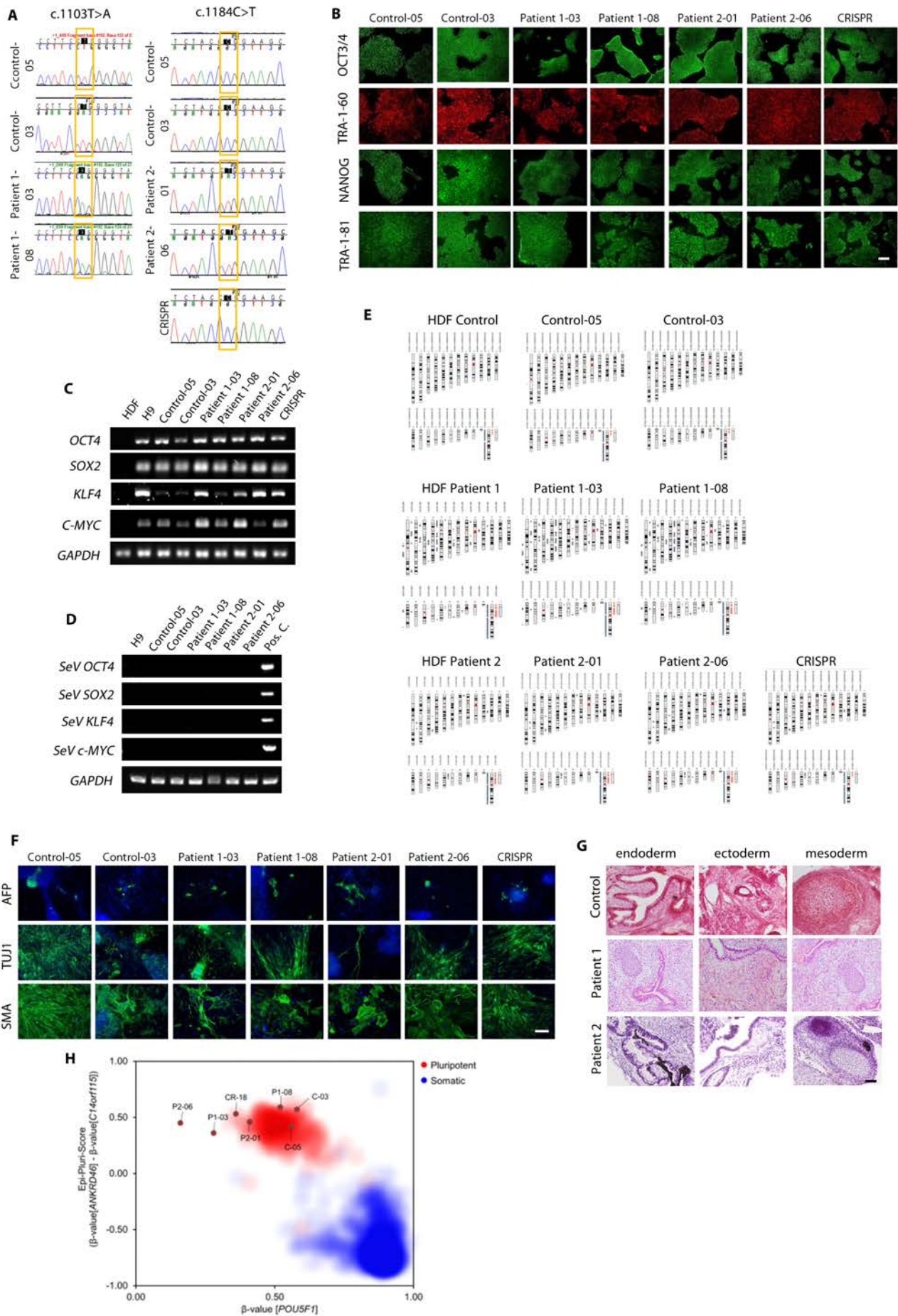
Knockout or wildtype breeding pairs were time-mated to generate knockout or wildtype litters. P0 pups were transcardially perfused and brains extracted on wet ice. The neonatal neurons were isolated using the Neural Dissociation Kit and MACS system Neuron isolation kit (Miltenyi Biotech) as per manufacturer's instructions. Neurons were seeded into poly-D-lysine coated coverslips in 12 well plates at density of 1×10^5 in 50 µl Neural basal medium (Invitrogen), 2% heat-inactivated fetal bovine serum (Sigma-Aldrich), 2% B27 supplement (Invitrogen), 200 mM L-glutamine (Sigma-Aldrich) and 25 mM L-glutamate (Sigma-Aldrich). Cells were rested for 30 minutes at 37°C and 450 µl of medium was added to each well. Cells were maintained in 5% CO₂ incubator at 37°C replacing 50% medium every 24 hours. Cultures were transduced on day 2 using AAV2.GFP or AAV2.hDAT at MOI 1000-10000 MOI in 5 µl media with 50% media replacement after 24 hours. On day 5, media was exchanged for phenol red free media collected on day 7. The cells were collected on day 7 for HPLC analysis, hDAT immunoblotting or immunofluorescence analysis as described above.

Vector genome transcript and qRT-PCR mRNA transcript expression analysis

Genomic DNA was recovered using the DNeasy Blood and Tissue kit (Qiagen) and quantified on Omega Fluostar. For the quantification of GFP or hDAT cDNAs transcripts, standardization was achieved by comparison against standard curves generated by amplification from plasmid constructs specific for GFP, hSLC6A3 and mGAPDH transcripts. This enabled estimation of absolute numbers of transcripts and reference GAPDH gene transcript, using a standard curve in Quantstudio Real-Time PCR System (Applied Biosystems).

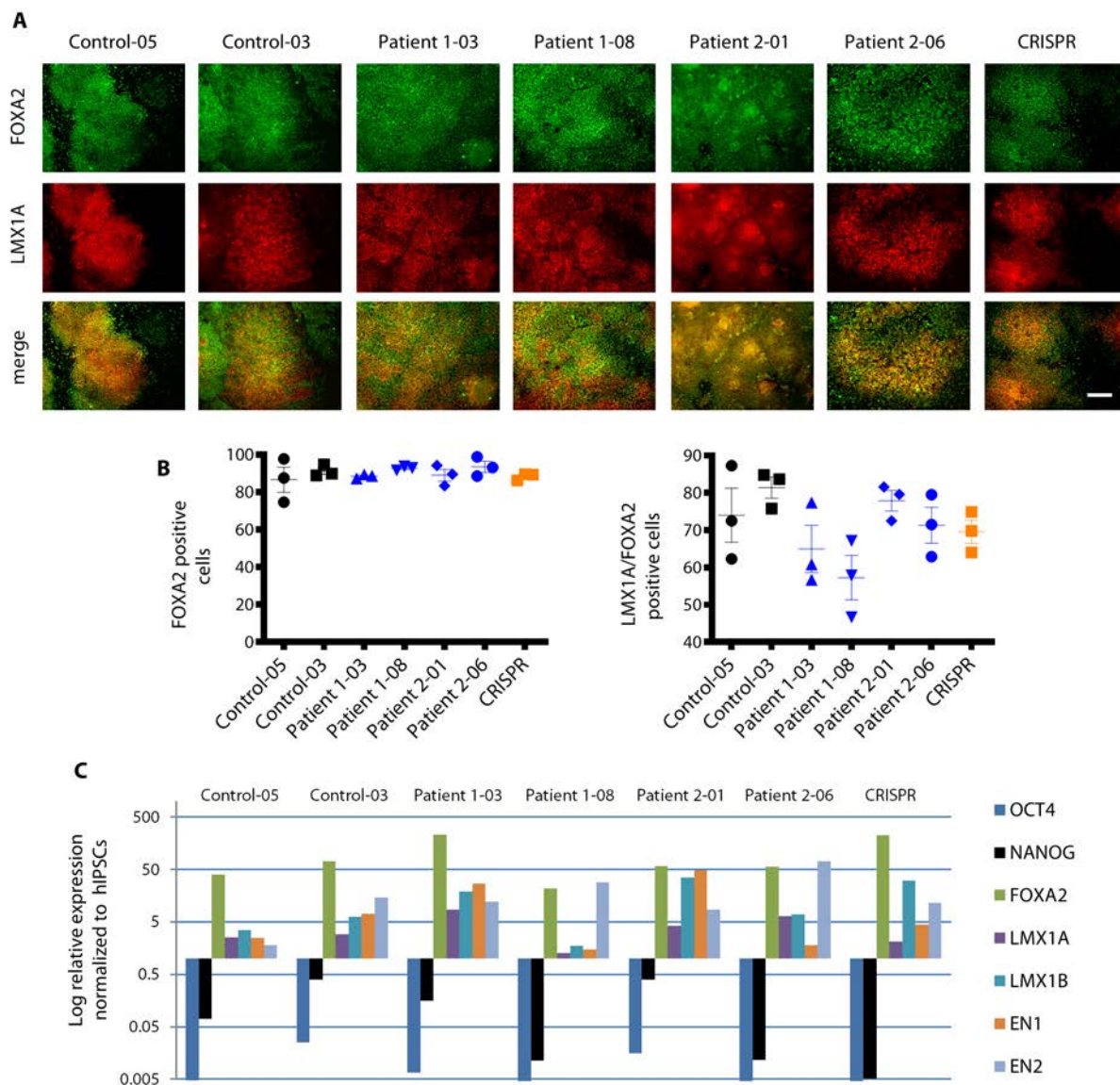
RNA was extracted from midbrain homogenate extracted with RNeasy mini kit (Qiagen) following the manufacturer's instructions and quantified on Omega Fluostar. Contaminating DNA was removed from total RNA (1 µg) using the DNase I purification kit (NEB), before performing reverse transcription with High-Capacity cDNA Reverse Transcription Kit (Applied Bioscience). Then 10 ng of DNA or synthesized cDNA was used to perform the multiplex hDAT and mGAPDH RT-qPCR with Luna Taqman mastermix (NEB) (Primers are listed Supplementary Table 4) in Quantstudio Real-Time PCR System (Applied Biosystems). GAPDH was used as endogenous controls and relative fold change calculated.

Supplementary Data



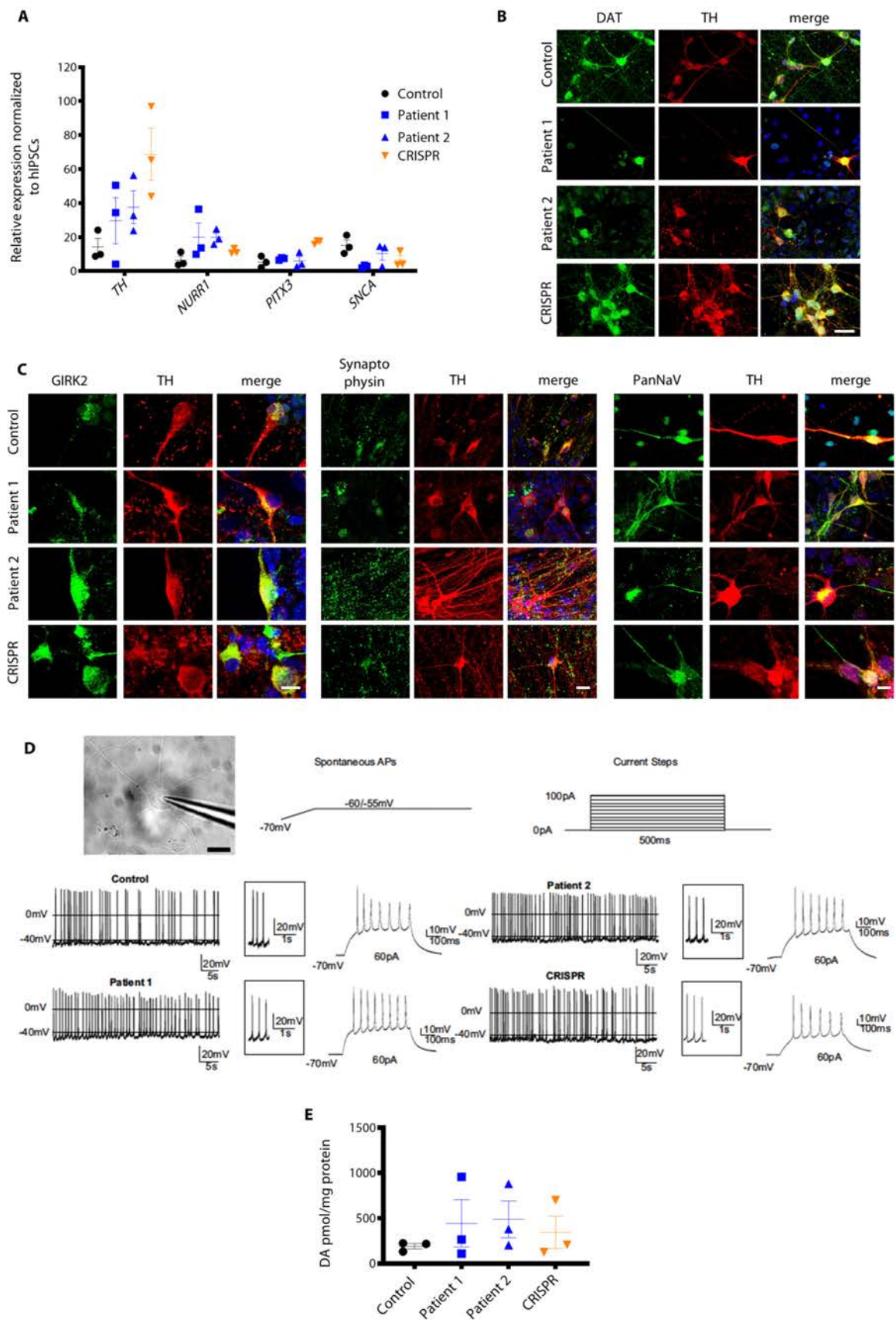
1 **Supplementary Figure 1: Generation of control patient and isogenic hiPSC lines**

2 **A** Sequence chromatograms showing c.1103T>A (p.L368Q) in Patient 1 lines Patient 1-03 and
3 Patient 1-08, absent in Control lines Control-05 and Control-03. Sequence chromatograms showing
4 c.1184C>T (p.P395L) in Patient 2 lines Patient 2-01 and Patient 1-06, absent in Control lines Control-
5 05 and Control-03, and the corresponding isogenic control line CRISPR. **B** Immunofluorescence
6 staining for pluripotency markers OCT3/4, TRA-1-60, NANOG, and TRA-1-81 in derived iPSC control
7 (Control-05, Control-03), Patient 1 (Patient 1-03, Patient 1-08), Patient 2 (Patient 2-01, Patient 2-06),
8 and isogenic control lines (CRISPR). Scale bar 200 µm. **C** RT-PCR for expression of pluripotency
9 genes *OCT3/4*, *SOX2*, *KLF4*, *C-MYC* in human dermal fibroblasts (HDF), human Embryonic Stem
10 Cells (H9) and derived iPSC lines. **D** RT-PCR for exogenous Sendai Virus genes (SeV): *OCT4*, *SOX2*,
11 *KLF4*, *c-MYC* in HDF, H9 and derived iPSCs. **E** Illumina Human OmniExpress24v1-0-a beadchip
12 analysis for original control (HDF Control) and patient (HDF Patient 1, HDF Patient 2) dermal
13 fibroblasts their respective derived iPSC lines (Control-05, Control-03 from HDF Control; Patient 1-
14 03, Patient 1-08 from HDF Patient 1; Patient 2-01, Patient 2-06 from HDF Patient 2). **F**
15 Immunofluorescence analysis of markers AFP (endoderm), TUJ1 (ectoderm) and SMA (mesoderm)
16 after 16 days of in vitro spontaneous differentiation of Control-05, Control-03, Patient 1-03, Patient 1-
17 08; Patient 2-01, Patient 2-06 and CRISPR human iPSC lines. Nuclei were stained for DAPI. Scale
18 bar 100 µm. **G** Teratoma from iPSCs derived from control and patient lines were generated after
19 subcutaneous injection of iPSC lines, and analyzed after isolation with haematoxylin and eosin.
20 Derivates of endoderm, ectoderm and mesoderm are observed in histological analysis. Scale bar 100
21 µm. **H** Assessment of pluripotency using Epi-Pluri-Score analysis. DNA-methylation was analyzed at
22 three specific CpG sites for both patient and control lines. Red and blue clouds refer to DNAm profiles
23 (Illumina HumanMethylation27 BeadChip platform) of 264 pluripotent and 1,951 non-pluripotent cell
24 preparations, respectively.



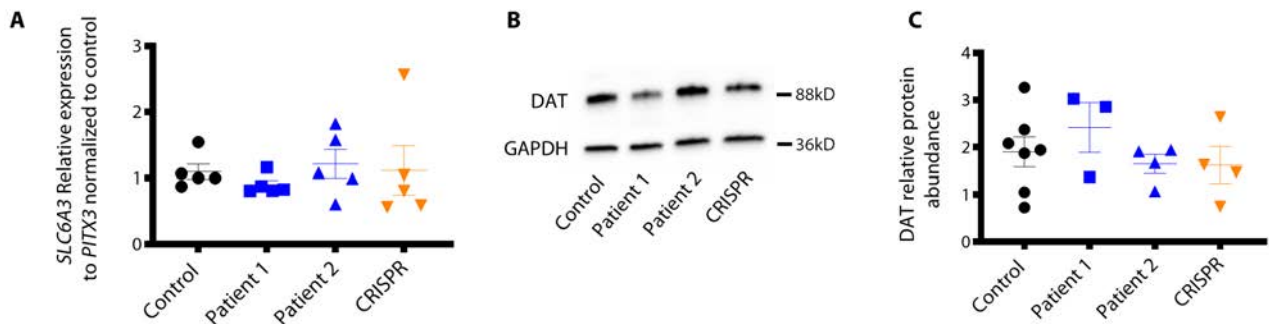
Supplementary Figure 2: Differentiation of control and patient iPSC lines into midbrain dopaminergic precursors

A Immunofluorescence analysis at d11 of mDA differentiation for the midbrain progenitor specific markers FOXA2 and LMX1A. Scale bar 200 μ m. **B** Differentiation efficiency analyzed after quantification of single FOXA2 positive cells and double LMX1A/FOXA2 positive cells differentiated from Control (Control-05, Control-03), Patient 1 (Patient 1-03, Patient 1-08), Patient 2 (Patient 2-01, Patient 2-06), and isogenic control lines (CRISPR) (n = 3 for each line). **C** qRT-PCR at d11 for pluripotency markers *OCT4* and *NANOG*, and midbrain related markers *FOXA2*, *LMX1A*, *LMX1B*, *EN1*, *EN2*, relative to housekeeping gene (*GAPDH*) and normalized to their respective iPSCs (n = 1 for each line). Error bars indicate SEM.



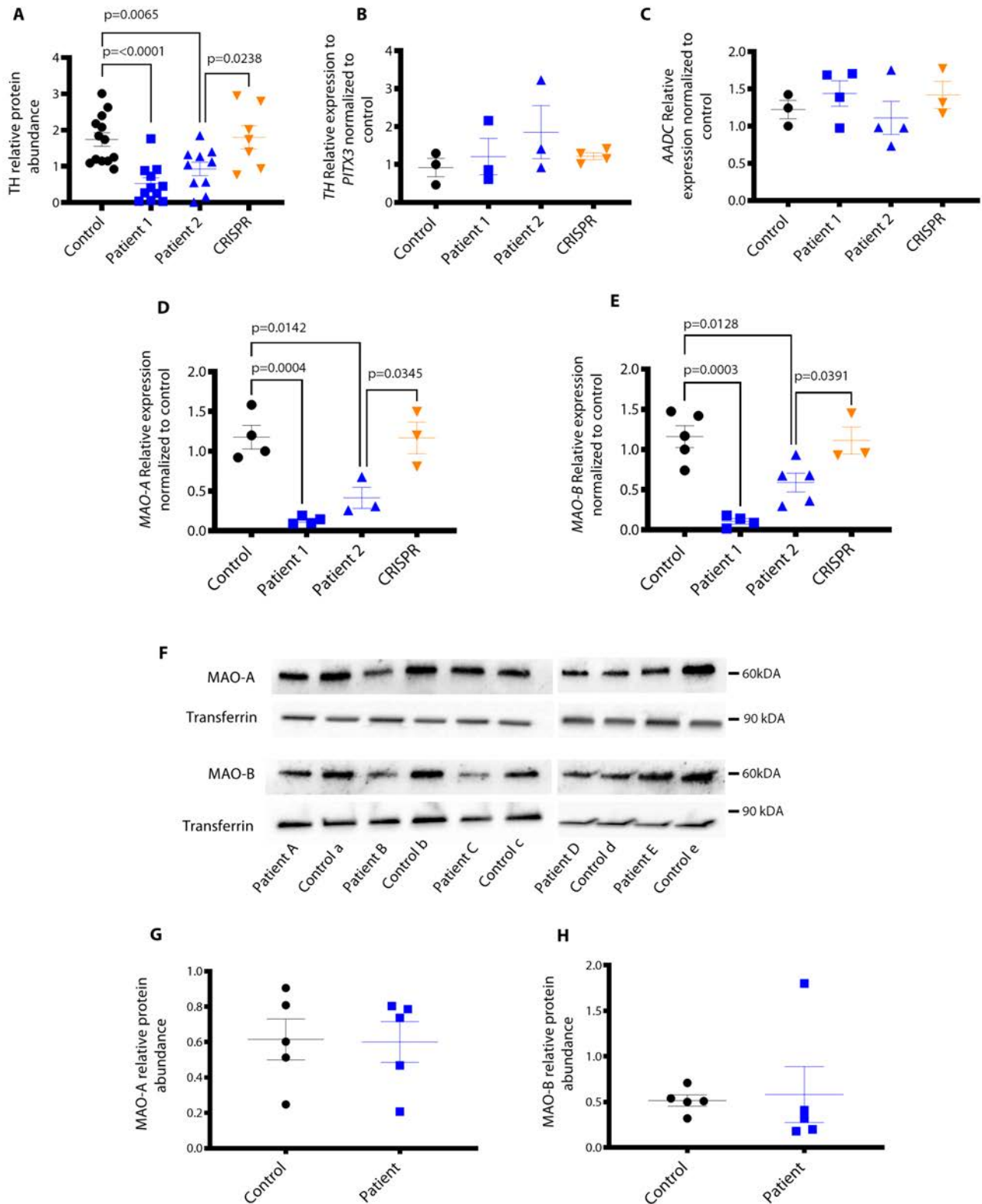
Supplementary Figure 3: Differentiation of control and patient neural progenitors into mature, electrically active mDA neurons

A qRT-PCR for *TH*, *NURR1*, *PITX3* and *SNCA* at d65. mRNA values are relative to the housekeeping gene and normalized to the corresponding hiPSCs (n = 3 per line). **B** Immunofluorescence analysis at d65 for TH and DAT. Nuclei are counterstained for DAPI. Scale bar 40 μ m. **C** Immunofluorescence analysis at d65 for TH, GIRK2, Synaptophysin and sodium voltage gated channels (PanNaV). Nuclei stained for DAPI. *Left* scale bar 10 μ m, *middle* scale bar 20 μ m, *right* scale bar 10 μ m. **D** Representative micrograph illustrating a patch pipette sealed to an iPSC-derived dopaminergic neuron, and schematic representation of the experimental protocols used for spontaneous APs and current steps injection (*upper line*). Representative current clamp traces (from n = 5/10 for each group, see Methods) for Control, Patient 1, Patient 2 and CRISPR. *Left*. Spontaneous repetitive APs recorded holding neurons at -60/-55 mV. *Right*. Representative traces of multiple APs elicited by current injection (60 pA) (*lower lines*). **E** HPLC detection of extracellular dopamine at d65 (n = 3 per line). Error bars indicate SEM.



Supplementary Figure 4: d65 DAT gene and protein expression profiles for control and patient lines

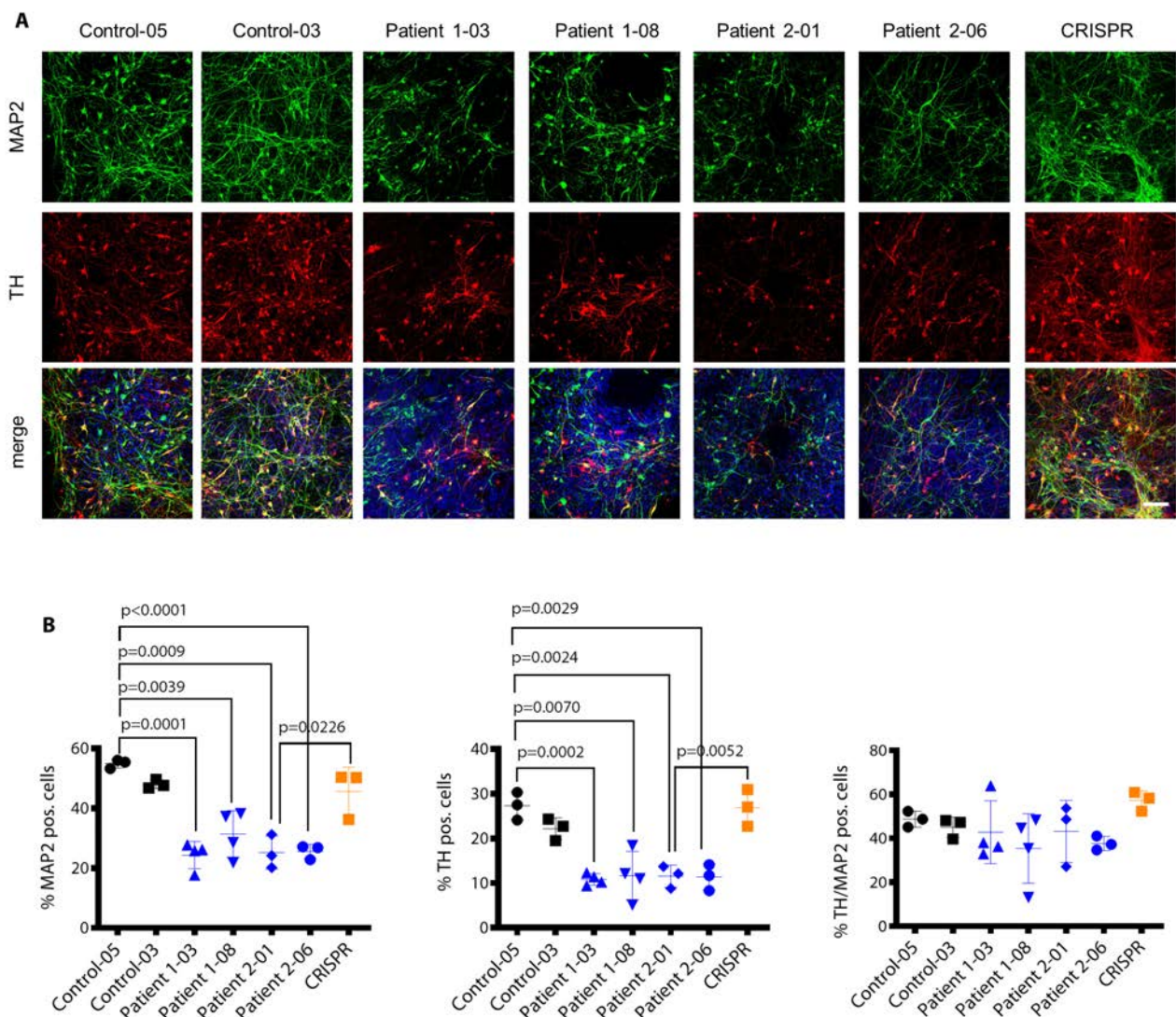
A Quantitative RT-PCR for SLC6A3 mRNA at d65 for Control, Patient 1, Patient 2 and CRISPR (n = 5 each). Values are relative to PITX3 and normalized to Control. **B** Immunoblot for DAT protein and loading control (GAPDH) from total cell lysates extracted at d65. **C** DAT protein abundance relative to GAPDH for Control, Patient 1, Patient 2 and CRISPR (n = 7, 3, 4, 4 respectively). Error bars indicate SEM. Both DTDS lines were independently compared to controls using two-tailed Student's *t*-test for all analyses.



1

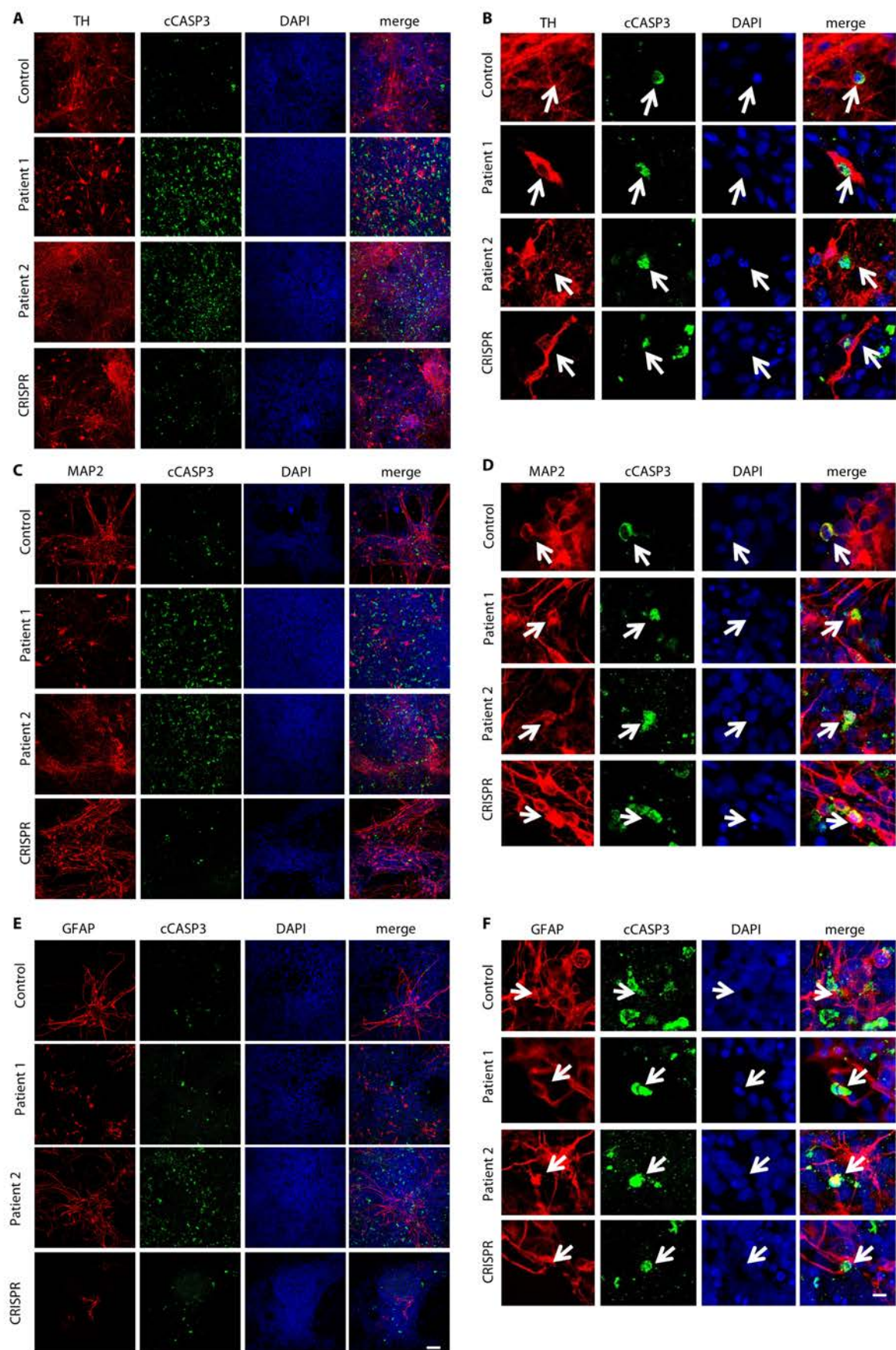
2 **Supplementary Figure 5: d65 gene expression profiles for key enzymes involved in dopamine**
 3 **metabolism in control and patient lines**

1 **A** Relative abundance of TH protein detected at d65 in Control, Patient 1, Patient 2 and CRISPR,
2 relative to housekeeping gene GAPDH (representative cropped blot Fig. 2A) (n = 13, 11, 10, 7
3 respectively). **B** *TH* expression in Control, Patient 1, Patient 2 and CRISPR derived mDA neurons at
4 d65. mRNA amount is relative to *PITX3* and normalized to Control (n = 3, 3, 3, 4 respectively). **C**
5 Quantitative RT-PCR for *AADC* expression in Control, Patient 1, Patient 2 and CRISPR at d65 relative
6 to housekeeping gene and normalized to Control (n = 3, 4, 4, and 3 respectively). **D** Quantitative RT-
7 PCR for *MAO-A* at d65. Values are relative to the housekeeping gene, and normalized to Control (n
8 = 4, 4, 3, 3 for Control, Patient 1, Patient 2 and CRISPR respectively). **E** Transcript content for *MAO-*
9 *B* measured by quantitative RT-PCR at d65 (n = 5, 4, 5, 3 for Control, Patient 1, Patient 2 and CRISPR
10 respectively). **F** Immunoblot for MAO-A/B and loading control (transferrin) from controls (Control a-b)
11 and patients (Patient A-E) CSF. **G, H** MAO-A and MAO-B respectively protein abundance relative to
12 transferrin for controls (Control; n = 5) and patients (Patients; n = 5). Error bars indicate SEM. Both
13 DTDS lines were independently compared to controls using two-tailed Student's *t*-test for all analyses.



Supplementary Figure 6: d65 quantification of mDA neurons in control and patient lines

A Immunofluorescence analysis at d65 for MAP2 and TH. Nuclei were counterstained with DAPI. Scale bar 100µm. **B** Quantification of the total number of MAP2-positive, TH-positive, and TH/MAP2 double-positive cells in control and patient lines ($n = 3, 3, 4, 4, 3, 3$ for Control-05, Control-03, Patient 1-03, Patient 1-08, Patient 2-01, Patient 2-06 and CRISPR respectively). Error bars indicate SEM. DTDS lines were independently compared to controls using two-tailed Student's *t*-test.

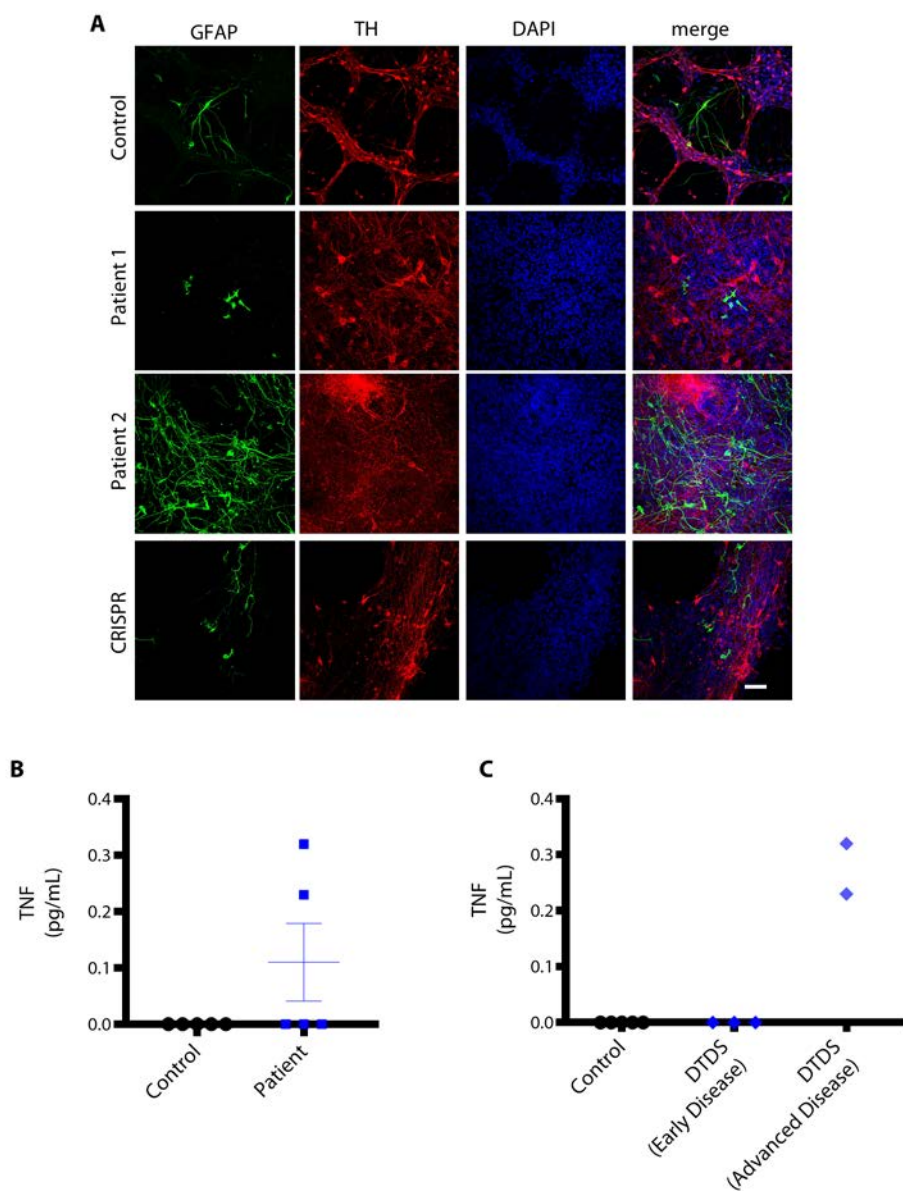


1 **Supplementary Figure 7: d65 immunofluorescence for cleaved caspase-3 (cCASP3) in control**
2 **and patient lines**

3 **A, C, E** Representative images of immunofluorescence analysis in mDA neurons at d65 for
4 TH/cCASP3, MAP2/cCASP3, and GFAP/cCASP3 respectively. Nuclei were stained with DAPI. Scale
5 bar 100 μ m. **B, D, F** Representative confocal images of immunofluorescence analysis for
6 TH/cCASP3, MAP2/cCASP3, and GFAP/cCASP3 in mDA neuronal populations at d65. Nuclei were
7 stained with DAPI. Arrows indicate double positive cells. Scale bar 10 μ m.

8

1



2

3 **Supplementary Figure 8: d65 immunofluorescence for GFAP in control and patient lines**

4 **A** Representative images of immunofluorescence staining for GFAP and TH in mDA neurons at d65.

5 Nuclei are stained with DAPI. Scale bar 100 μ m. **B** CSF cytokine analysis for TNF in controls and

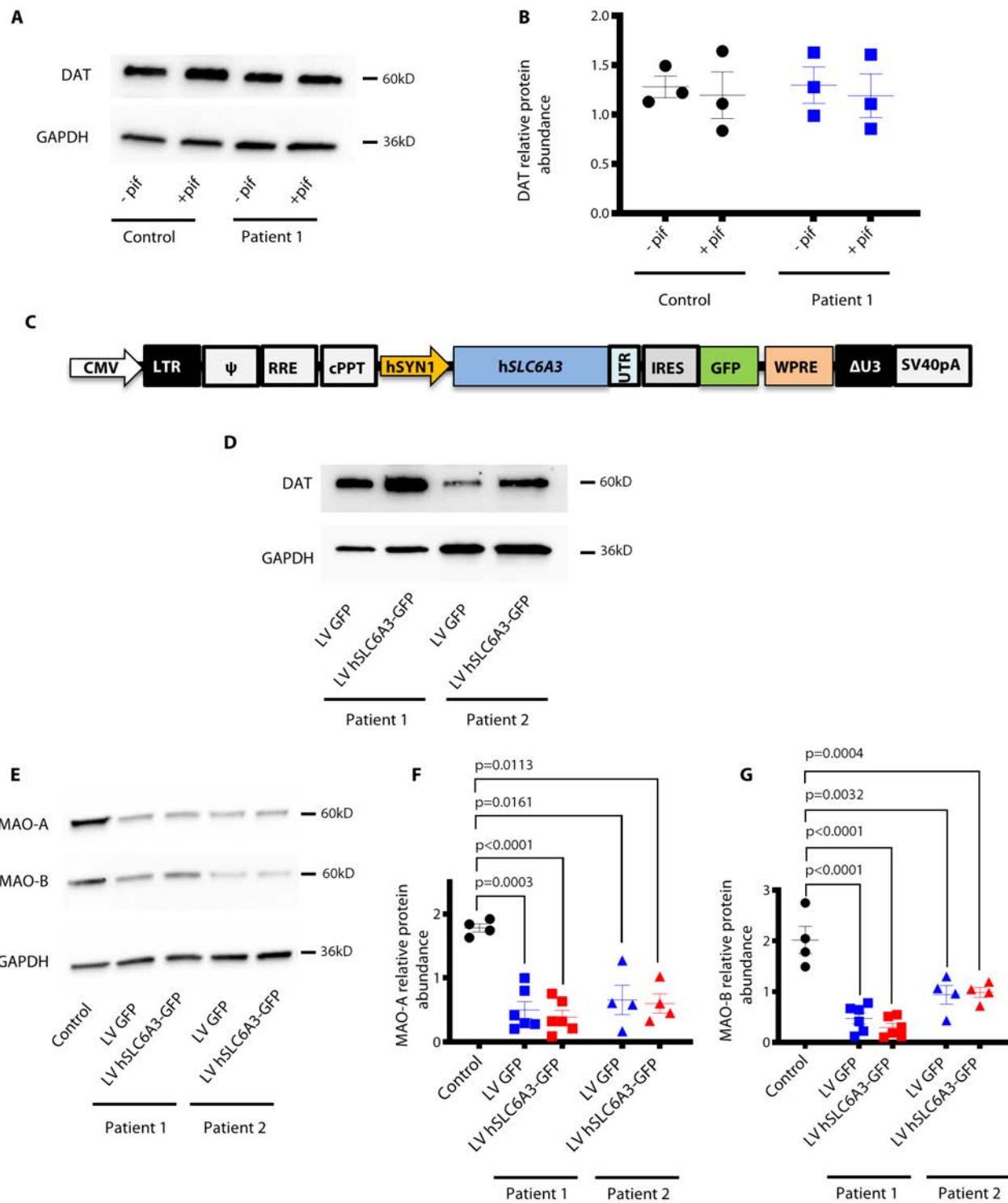
6 Patients with DTDS (n = 5 for both). Error bars indicate SEM. Two-tailed Student's t-test. **C** Analysis

7 of TNF concentration in CSF of controls (n = 5), Patients with DTDS with early disease (DTDS Early

8 Disease), age at CSF acquisition < 2 years (n = 3) and advanced disease (DTDS Advanced Disease),

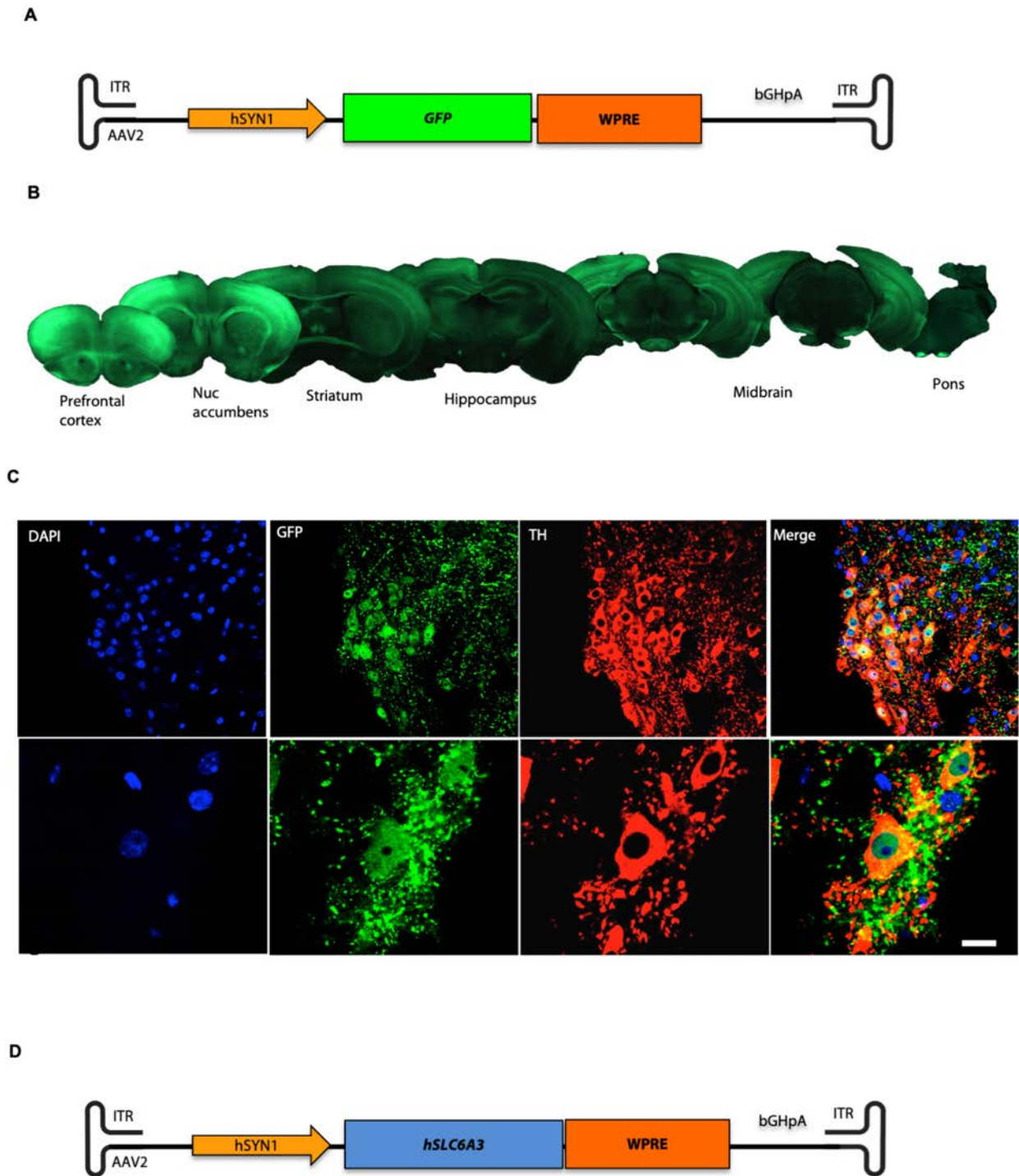
9 age at CSF acquisition 6 and 16 years (n = 2).

10



Supplementary Figure 9: Therapeutic approaches for DTDS with pifithrin- μ and lentiviral gene transfer in the mDA neuronal model

A Cropped immunoblot of total DAT and GAPDH in Control and Patient 1 mDA neurons at d65. Culture were treated for 24h with Pifithrin- μ (pif). **B** Quantification of DAT protein relative to GAPDH in control and patient-derived neurons (n = 3 per line). **C** Schematic representation of lentiviral construct utilized for in vitro gene transfer with expression cassette containing human synapsin promoter (hSyn1) driving human *SLC6A3* gene (h*SLC6A3*) linked by Internal Ribosome Entry Site sequence (IRES) and GFP gene (not drawn to scale). **D** Cropped immunoblot of total DAT and GAPDH in Patient 1 and Patient 2 -derived mDA neurons transfected with either a lentivirus construct expressing GFP alone (LV GFP) or human *SLC6A3* and GFP (LV h*SLC6A3*-GFP). **E** Cropped immunoblot for total MAO-A, MAO-B and GAPDH in neuronal culture at d65 from Control, Patient 1 and Patient 2. Patient-derived neurons were transfected with GFP or h*SLC6A3*-GFP lentivirus constructs. **F,G** Quantification of MAO-A and MAO-B protein relative to GAPDH in control and patients-derived neurons transfected with GFP or h*SLC6A3*-GFP lentivirus constructs (n = 4, 6, 6, 4, 4 for each condition/line and for both protein quantification). Both DTDS lines were independently compared to controls using two-tailed Student's *t*-test for all analyses.

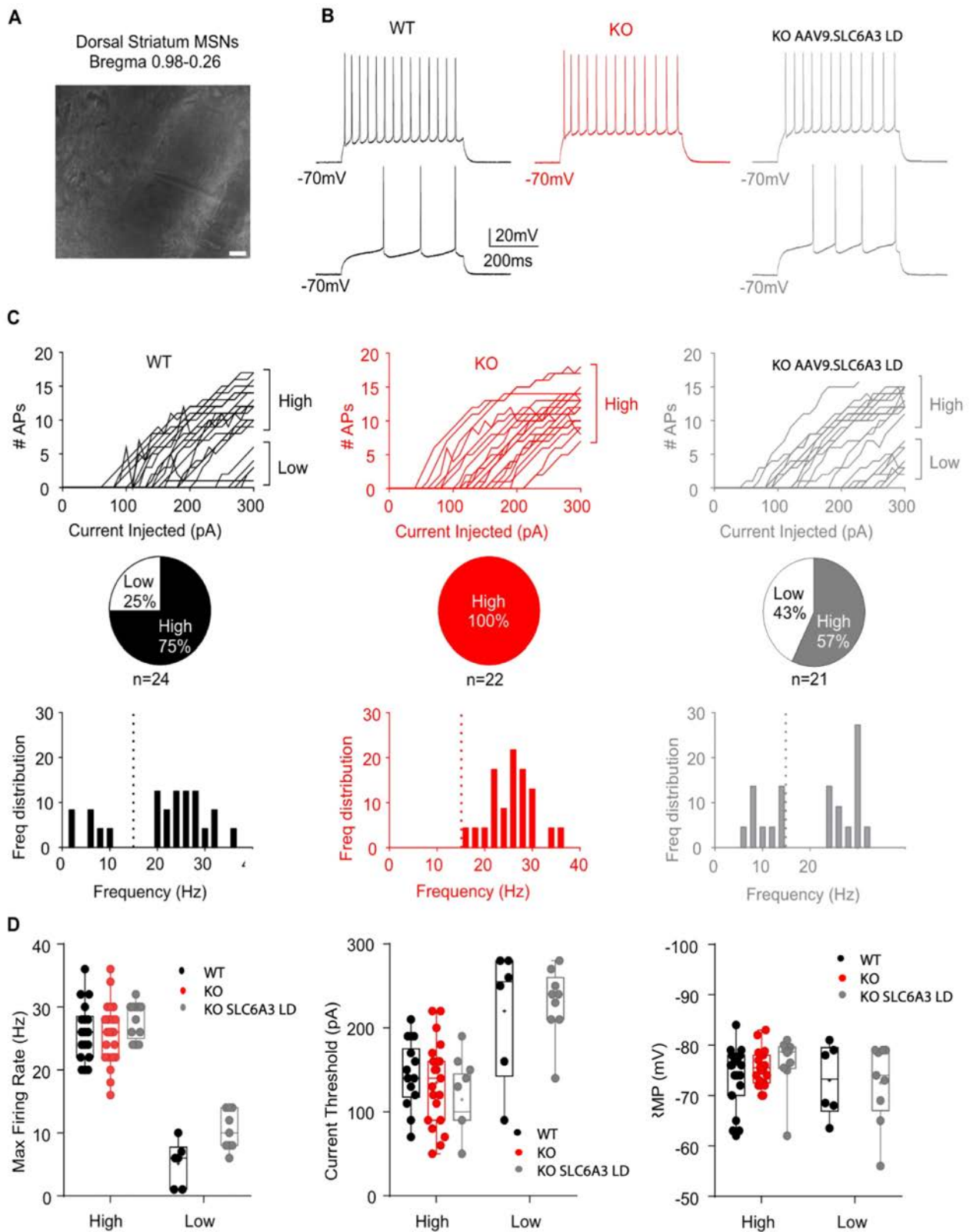


Supplementary Figure 10: In vivo AAV9 hSyn GFP marker gene study.

A Illustration of p.AAV.GFP plasmid expression cassette used to for in vivo gene transfer to assess brain and mDA neuronal transduction. The expression cassette contains a truncated hSyn1 promoter driving GFP expression followed by a Woodchuck Hepatitis Virus Posttranscriptional Regulatory Element and bGH polyadenylation signal flanked by AAV2 derived ITR (not to scale).

1 **B** Representative GFP immunofluorescence of brain sections from prefrontal cortex to pons following
2 intracerebroventricular delivery of AAV9.hSyn.GFP vector to neonatal wildtype mice and brain tissue
3 collected at P35. Representative of 4 animals. **C** Representative images of double labelled GFP and
4 TH positive mDA neurons transduced with AAV9.hSyn.GFP following neonatal
5 Intracerebroventricular delivery (scale bar 100µm, n = 4 animals). **D** Illustration of p.hSyn.SLC6A3
6 expression cassette generated for in vivo gene therapy experiments. The expression cassette
7 contains a truncated hSyn promoter driving hSLC6A3 expression followed by a Woodchuck Hepatitis
8 Virus Posttranscriptional Regulatory Element and bGH polyadenylation signal flanked by AAV2

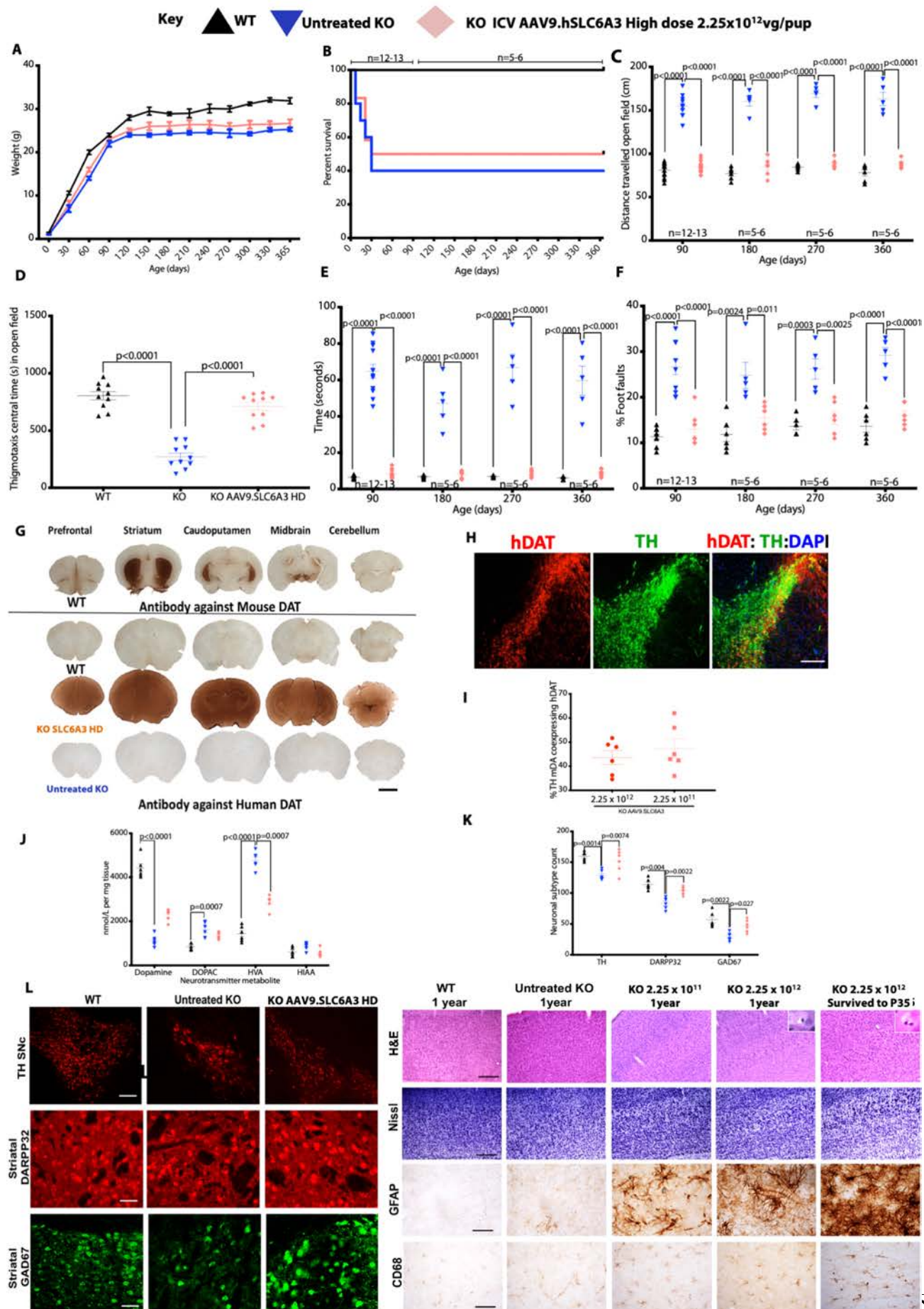
1 derived ITR (not to scale).



2

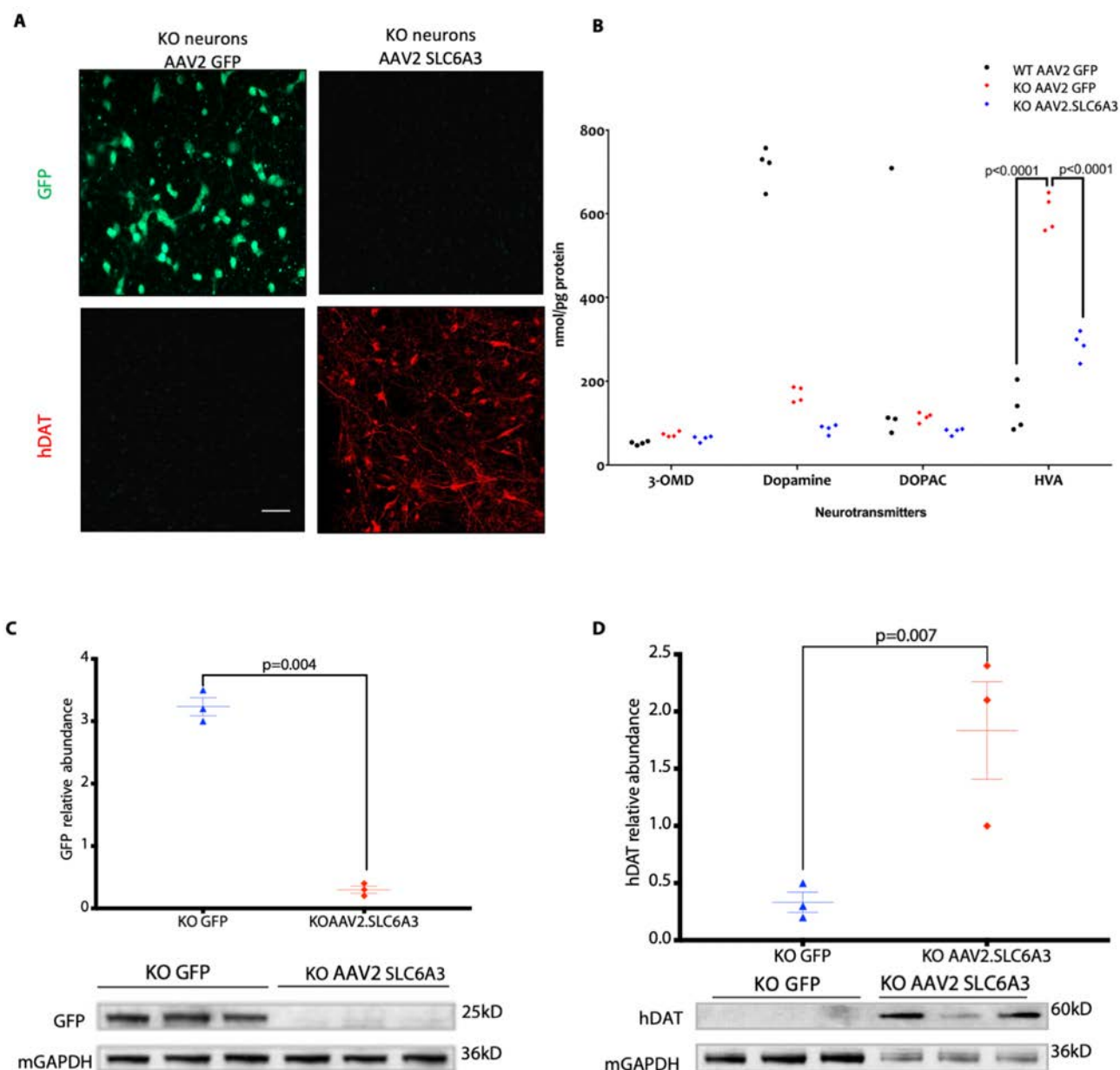
1 **Supplementary Figure 11: Electrophysiological properties of Medium Spiny Neurons following**
2 **neonatal AAV9.hSLC6A3 gene therapy**

3 **A** Current clamp recordings were performed on visually identified Medium Spiny Neurons in the dorsal
4 striatum (Bregma 0.98-0.5; Scale bar 10 μ m) from AAV9.hSLC6A3 low dose treated knockout,
5 wildtype and untreated knockout mice (n = 3 animals per group, a range 9 - 11 neurons were recorded
6 per animal). **B** Representative traces of APs elicited by 300 pA current injection in wild-type (black
7 traces), untreated knockout (red trace) and knockout hDAT (grey traces). Wildtype and knockout
8 hDAT showed two different populations of Medium Spiny Neurons while knockout only the one more
9 excitable. **C** Top. Number of APs vs injected current for all the experimental data: wild-type (black n
10 = 24), untreated knockout (red n = 22) and knockout AAV9.hSLC6A3 low dose (grey n = 21). Middle.
11 Percentage of high and low firing frequency in the 3 experimental groups. Bottom. Frequency
12 distribution (%) of the firing rate for wild-type (black), untreated knockout (red) and knockout hDAT
13 (grey). **D** Maximum firing rate, Current threshold and RMP showed as mean \pm SEM for wild-type,
14 untreated knockout and knockout AAV9.hSLC6A3 LD divided for high and low frequency firing rate.



Supplementary Figure 12: AAV9.hSLC6A3 intracerebroventricular gene transfer at higher dosage

A Weights of mice 2.25×10^{11} vg/pup intracerebroventricular treated knockout $n = 12$, wildtype $n = 12$, untreated knockout $n = 17$ (Data means \pm S.E.M.) **B** Kaplan-Meier survival plot of wildtype, untreated knockout, intracerebroventricular higher dosage AAV9.hSLC6A3 treated knockout (Logrank, Mantel-Cox test). **C** Locomotor assessment of mice in open field with distance travelled **D** thigmotaxis central time **E** vertical pole descent time **F** foot faults (Data means \pm S.E.M., two-way ANOVA, Log transformed data for % foot fault, Bonferroni's multiple comparison, group sizes as stated). **G** Representative immunostaining for mouse DAT in wildtype mice for physiological expression reference. Immunostaining for human DAT in treated knockout, untreated knockout and wildtype mice (scale bar 1 mm, $n = 5$ per group). **H** Representative image of double labelled immunofluorescence for % TH positive mDA co-expressing hDAT in knockout mice treated with higher dose AAV9.hSLC6A3 2.25×10^{11} vg/pup (scale bar 250 μ m, $n = 6$ per group). **I** Quantification of co-expressing cells from knockout AAV9.SLC6A3 treated with high and low dosage group (Data means \pm S.E.M. $n = 6$ per group, no significant difference on Student's *t*-test). **J** Dopamine and serotonin neurotransmitter metabolites from whole brain homogenates analyzed by HPLC (numbers of animals stated, two-way ANOVA, Bonferroni's multiple comparison). **K** Neuronal counts of TH, DARP32 and GAD67 positive neuronal subtypes from midbrain and striatal sections in wild-type, untreated knockout and high dose treated knockout at 356 days ($n = 6$ animals per group, two-way ANOVA, Tukey's multiple comparison). **L** Representative images of immunofluorescence of mDA TH neurons (scale bar 250 μ m) and striatal DARP32 and GAD67 neurons (scale bar 100 μ m) from wildtype, untreated knockout and higher dose treated knockout ($n = 6$ per group). **M** Neurohistological panel of brain cortex of wildtype, untreated knockout and knockout hDAT treated mice at lower dosage at 1 year. Knockout mice treated with 10 fold higher dosage showed 50 % survival and were analyzed at 1 year and those with reduced survival at P35. Representative images of Haematoxylin and Eosin and Nissl stain (scale bar 0.25 mm), immunohistochemistry for GFAP and CD68 (scale bar 100 μ m) of frontal cortex. ($n = 5 - 6$ animals per group).



Supplementary Figure 13: AAV2.hSLC6A3 in vitro transduction of knockout primary neurons

A Representative immunocytofluorescence for GFP and hDAT expression on knockout primary neurons harvested by P2 cortical dissociation transduced with AAV2.GFP or AAV2.hSLC6A3 vector MOI 1:10000 (scale bar 100 μ m) n = 6 per group. **B** Dopamine metabolite HPLC analysis of neuronal cell lysates of knockout primary neurons transduced with AAV2.hSLC6A3 and knockout and wildtype primary neurons transduced with AAV2.GFP served as controls (MOI 10000) (Data means \pm S.E.M., two-way ANOVA n = 4 per group). **C** upper panel Quantification of GFP protein from knockout neuronal cell lysates transduced with AAV2.GFP or AAV2.hSLC6A3 normalized to loading control mGAPDH (Data means \pm S.E.M. Student's t-test n=3 per group). Lower panel corresponding

immunoblot for GFP and mGAPDH **D** upper panel Quantification hDAT protein from knockout neuronal cell lysates transduced with AAV2.GFP or AAV2.hSLC6A3 normalized to loading control mGAPDH (Data means \pm S.E.M. *Student's t-test* $n=3$ per group). Lower panel corresponding immunoblot for GFP and mGAPDH.

Supplementary Figure 14: AAV2.hSLC6A3 stereotactic gene delivery to substantia nigra

A Schematic of AAV2.hDAT gene delivery to 4 weeks old mice by midbrain stereotactic injection. **B** Open field trajectory traces of all animals injected with AAV2.hDAT vector treated knockouts at 3 dosages 2×10^{10} , 2×10^9 , 2×10^8 vg/mouse. Control wildtype and knockout animals received AAV2.GFP vector 2×10^{10} vg/mouse. Behavioral testing performed at 12 weeks old (8 weeks post injection, $n = 5 - 8$ per group). **C** Quantification of TH neurons co-expressing human DAT in knockouts treated with AAV2.hDAT 2×10^{10} , 2×10^9 , 2×10^8 vg/mouse (Data means \pm S.E.M. two-way ANOVA, Tukey post hoc analysis, $n = 3$ per group). **D** qRT-PCR was used to quantify hSLC6A3 mRNA transcripts in 40 μ m midbrain slice from wildtype and knockout AAV2.GFP treated mice and knockouts treated with AAV2.hSLC6A3 at 2×10^{10} vg, 2×10^9 vg, 2×10^8 vg/mouse. mGAPDH was used for normalisation and calculate fold change from GFP injected mice. (Data means \pm S.E.M. two-way ANOVA, Tukey post hoc analysis, $n = 3$ per group) **E** Total genomic DNA from 40 μ m midbrain slice from knockout mice treated AAV2.hDAT as dosages 2×10^{10} , 2×10^9 , 2×10^8 vg/mouse was analyzed by qPCR to calculate Vector genome copies (vgc) (Data are means \pm SEM, two-way ANOVA, $n = 3$). **F** upper panel Quantification of MAO-A protein from tissue lysate of 40 μ m midbrain slice from wildtype and knockout mice treated with AAV2.GFP 2×10^{10} vg/mouse and knockouts treated with AAV2.hDAT 2×10^{10} vg/mouse (Data means \pm S.E.M. two-way ANOVA, Tukey post hoc analysis, $n = 3$ per group). Lower panel corresponding Immunoblot of MAO-A protein from tissue lysate from 40 μ m midbrain slice with loading control mGAPDH. **G** upper panel Quantification of MAO-B protein from tissue lysate of midbrain tissue from wildtype and knockout mice treated with AAV2.GFP 2×10^{10} vg/mouse and knockouts treated with AAV2.hSLC6A3 2×10^{10} vg/mouse (Data means \pm S.E.M. two-way ANOVA, Tukey post hoc analysis $n = 3$ per group). Lower panel corresponding Immunoblot of MAO-B from midbrain slice with loading control mGAPDH.

1 Supplementary Tables

2 Supplementary Table 1: Primers for CRISPR correction of *SLC6A3* variant c.1184C>T

Primer	Sequence
DAT.g4	TAGATGATGAAGATCAGCCCTGG
DAT.g5	GGACAGAGGGAGCGTGGCGATGG
DAT-GT-F	CCCAAAAGGACCCAGGTAAT
DAT-GT-R	TCCAGTCACCACTCACTCCA

3 Supplementary Table 2: List of antibodies

Name	Use, concentration	Source, catalogue number
AADC	WB, 1:5000	Thermo Scientific, PA5-25450
AFP	IC, 1:100	Sigma-Aldrich, WH0000174M1
alpha smooth muscle	IC, 1:300	Abcam, ab32575
Cleaved Caspase-3	IF, 1:400	Cell Signaling Tech., Asp175
COMT	WB, 1:3000	Abcam, ab126618
DAT	IC/IHC, 1:100/1000	Millipore, MAB369
DAT	WB/IF, 1:3000/500	Millipore, AB1766
FOXA2	IC, 1:500	BD Pharmigen, 561580
GAPDH-HRP	WB, 1:3000	Cell Signaling Tech, 3683
GFAP	IC/IHC 1:400/500	Millipore, MAB3402
GFP	IHC, 1:10000	Abcam, AB290
GFP	IC/IF 1:500	Aves Labs, GFP-1010
GIRK2	IC, 1:400	Alomone Labs, APC-006
LMX-1	IF, 1:2000	Millipore, AB10533
MAO-B	WB, 1:1000	Abcam, ab133270
MAO-A-HRP	WB, 1:3000	Abcam, ab200928
MAP2	IC, 1:400	Sigma-Aldrich, M9942
NANOG	IF, 1:500	Millipore, MABD24
Oct3/4	IC, 1:400	Santa Cruz Biotech, sc-5279
Pan-NaV	IC, 1:50	Sigma-Aldrich, S8809
Synaptophysin	IC, 1:400	Sigma-Aldrich, SAB4502906

TH	IC/IF 1:400/500	Aves Labs, TYH
TH	WB/IF 1:3000/1000	Millipore, AB152
TRA-1-60	IC, 1:400	Santa Cruz Biotech., sc21705
TRA-1-81	IF, 1:200	Millipore, MAB4381
TUJ1	IC, 1:400	Biolegend, MMS-435P

- 1 IC:immunocytochemistry. WB: western blotting, IHC: immunohistochemistry, IF:
- 2 immunofluorescence

3 **Supplementary Table 3: Primers sequences**

	Primer forward sequence	Primer reverse sequence	Use
AADC	TGCGAGCAGAGAGGGAGTAG	TGAGTTCCATGAAGGCAGGATC	qRT-PCR
c-MYC	GCGTCCTGGGAAGGGAGATCCGGAGC	TTGAGGGGCATCGTCGCGGGAGGCTG	RT-PCR
COMT	TGAACGTGGGCGACAAGAAAGGCAAGAT	TGACCTTGTCTTCACGCCAGCGAAAT	qRT-PCR
DAT	TCACCAACGGTGGCATCTAC	CACTCCGATGGCTTCGATGA	qRT-PCR
DAT	TCGTCGTCTTCTCCTTCCTG	GATGGCTTCCGGGTAGATGA	qRT-PCR
EN1	CGTGGCTTACTCCCCATTTA	TCTCGCTGTCTCTCCCTCTC	qRT-PCR
EN2	CCTCCTGCTCCTCCTTCTT	GACGCAGACGATGTATGCAC	qRT-PCR
FOXA2	CCGTTCTCCATCAACAACCT	GGGGTAGTGCATCACCTGTT	qRT-PCR
GAPDH	ATCCCATCACCATCTTCCAG	CCATCACGCCACAGTTTCC	RT-PCR
GAPDH	TTGAGGTCAATGAAGGGGTC	GAAGGTGAAGGTCGGAGTCA	qRT-PCR
KLF4	ACGATCGTGGCCCCGAAAAGGACC	TGATTGTAGTGCTTCTGGCTGGGCTCC	RT-PCR
LMX1A	CGCATCGTTTCTTCTCCTCT	CAGACAGACTTGGGGCTCAC	qRT-PCR
LMX1B	CTTAACCAGCCTCAGCGACT	TCAGGAGGCGAAGTAGGAAC	qRT-PCR
MAO-A	CTGATCGACTTGCTAAGCTAC	ATGCACTGGATGTAAAGCTTC	qRT-PCR
MAO-B	GCTCTCTGGTTCCTGTGGTATGTG	TCCGCTCACTCACTTGACCAGATC	qRT-PCR
mouseGAPDH	ACGGCAAATTCAACGGCAC	TAGTGGGGTCTCGCTCCTGG	qRT-PCR
NANOG	TTGGGACTGGTGAAGAATC	GATTTGTGGCCTGAAGAAA	qRT-PCR
NURR1	TCGACATTTCTGCCTTCTCCTG	GGTTCCTTGAGCCCGTGTCT	qRT-PCR
OCT3/4	CGAAACCCACACTGCAGCAG	CCTGGCACAACTCCAGGTTT	RT-PCR
OCT3/4	TCTCCAGGTTGCCTCTCACT	GTGGAGGAAGCTGACAACAA	qRT-PCR
PITX3	GAGCTAGAGGCGACCTTCC	CCGGTTCTTGAACCACACCC	qRT-PCR
SNCA	GGAGTGGCCATTGACGAC	CCTGCTGCTTCTGCCACAC	qRT-PCR
SOX2	GGGAAATGGGAGGGGTGCAAAGAGG	TTGCGTGAGTGTGGATGGGATTGGTG	RT-PCR
TH	CGGGCTTCTCGGACCAGGTGTA	CTCCTCGGCGGTGTACTCCACA	qRT-PCR

4

5

1 **Supplementary Table 4:** Primers sequences used in generation of vector expression cassette, viral
2 vector titration and qRT-PCR

Primer	Sequence	Use
1F	CGAGACTAGCCTCGAGCGCGCTCTCTTAAGGTAGC	Cloning
1R	GAGGTTGATTGTGACGCTGGATGGGACAACAACG	Cloning
2F	CCCATCCAGCGTCGACGACGAGTTCTTCTGAGCGG	Cloning
2R	GAGGTTGATTGTGACGAGGCCGCTTTACTTGTAC	Cloning
3F	GGGCACACTGGGAGTTGAGGAATTCCACCACA	Cloning
3R	TCCCAGTGTGCCCGATCCGATGGTGAGCAAGGGC	Cloning
3F, MH531	TGTGTGCCCCGTCTGTTGTGT	LVV titration
3R, MH532	GAGTCCTGCGTCGAGAGAGC	LVV titration
Probe	(FAM)-CAGTGGCGCCCGAACAGGGA-(BHQ_1)	LVV titration
LVGFPP	ACTCCCAGTGTGCCCATGGTGAGCAAGGGCGAGGAGCTGT	Cloning
LVGFPR	GCCCTTGCTCACCATGGGCACACTGGGAGTTGAGGAATTCCAC	Cloning
GFPP	GGCACAAGCTGGAGTACAAC	Titration, RT-qPCR
GFPR	AGTTCACCTTGATGCCGTTT	Titration, RT-qPCR
GFP Probe	(FAM) AGCCACAACGTCTATATCATGGCCG	Titration, RT-qPCR
hDATF	TCGTCGTCTTCTCCTTCCTG	RT-qPCR
hDATR	GATGGCTTCCGGGTAGATGA	Titration, RT-qPCR
hDAT Probe	(FAM) ACACTGTGCTTCTGTGCCATGTACC	Titration, RT-qPCR
mGAPDH	ACGGCAAATTCAACGGCAC	RT-qPCR
mGAPDH	TAGTGGGGTCTCGCTCCTGG	RT-qPCR
mGAPDH Probe	(VIC)TTGTCATCAACGGGAAGCCCATCA	RT-qPCR

3 **Supplementary movies**

4 **Supplementary movie 1 legend:**

5 Untreated DAT knockout showing classical hyperlocomotor behaviour at P21 with three wildtype
6 littermates.

7 **Supplementary movie 2 legend:**

8 Untreated DAT knockout showing tremor, bradykinesia, hunched and piloerect at P35.

9 **Supplementary movie 3 legend:**

1 Open field locomotor activity of male DAT knockout treated AAV9.hSLC6A3 with untreated male
2 knockout littermate at 365 days. Untreated DAT knockout shows classical hyperlocomotor activity.

3 **Supplementary movie 4 legend:**

4 Open field locomotor activity of male DAT knockout treated with ten-fold higher dosage AAV hDAT
5 with untreated male knockout littermate at 365 days. Untreated DAT knockout showing
6 hyperlocomotor activity.

7

8 **Supplementary movie 5 legend:**

9 Open field locomotor activity of 12 weeks old adult mice treated with AAV2. GFP treated wildtype,
10 knockout mice and AAV2.hSLC6A3 treated knockout at 2×10^{10} vg/mouse.

11

12 **Supplementary movie 6 legend:**

13 Open field locomotor activity of adult DAT knockout mice treated with AAV2.hSLC6A3 vector at neat
14 $= 2 \times 10^{10}$, 1:10 = 2×10^9 and 1:100 = 2×10^8 vg/mouse dosages.

15

16

17